

A DEEP WIDE-FIELD VARIABLE STAR CATALOG OF ω CENTAURI

DAVID T F WELDRAKE

Max Planck Institut Für Astronomie, Königstuhl 17, D-69117, Heidelberg, Germany
weldrake@mpia-hd.mpg.de

PENNY D SACKETT

Research School of Astronomy and Astrophysics, Australian National University, Mount Stromlo
Observatory, Cotter Road, Weston Creek, ACT 2611, Australia
Penny.Sackett@anu.edu.au

TERRY J BRIDGES

Physics Department, Queen's University, Kingston, Ontario, Canada K7L 3N6
tjb@astro.queensu.ca

Draft version October 21, 2018

ABSTRACT

We present a variable star catalog of an extensive ground-based wide-field variability survey in the globular cluster ω Centauri. Using the ANU 40-inch (1m) telescope at Siding Spring Observatory, the cluster was observed with a $52' \times 52'$ (0.75 deg^2) field for 25 nights. A total of 187 variable stars were identified in the field, 81 of which are new discoveries. This work comprises the widest field variability survey yet undertaken for this cluster. Here we present the V+R lightcurves and preliminary analysis of the detected variable stars, comprising 58 eclipsing binaries, 69 RR Lyrae stars, 36 long period variables ($P \geq 2\text{d}$) and 24 miscellaneous pulsators including 15 SX Phoenicis stars and two Type II Cepheids.

Analysis of the eclipsing binary radial distribution has revealed an apparent lack of binaries in the $8' - 15'$ range, perhaps indicating two separate binary populations. Four detached binaries have short periods ($< 2.5\text{d}$) and are likely composed of low-mass M-dwarf components, useful for testing stellar evolution models. One further detached system has a period of 0.8 days and due to the blueness of the system could be composed of white dwarf stars. Analysis of the RR Lyrae sample has produced a reddening corrected distance modulus (also accounting for metallicity spread) for the cluster of 13.68 ± 0.27 , a result consistent with previously published values. This paper also presents a total stellar database comprising V and I photometry (with astrometry better than $0.25''$) for 203,892 stars with $12.0 \leq V \leq 21.0$ and 25-night V+R lightcurves for 109,726 stars ($14.0 \leq V \leq 22.0$) for both the cluster and the field.

Subject headings: globular clusters: individual ω Centauri (NGC 5139) — binaries: eclipsing — binaries: general — stars: variables: Delta Scuti — other

1. INTRODUCTION

Omega Centauri (ω Cen) has been the subject of intense interest over the years, as it possesses several distinctive features that differentiate it significantly from other members of the Galactic globular cluster system. Firstly, it is the most massive of the globular clusters, with a total absolute visual magnitude of -10.29 (Harris 1996), comparable to low-mass dwarf galaxies. The cluster possesses a high internal rotation velocity of $\sim 8 \text{ km/s}^{-1}$, (Merritt et al. 1997) with a central one-dimensional velocity dispersion of $\sim 15 - 20 \text{ km/s}^{-1}$ (Meylan & Mayor 1986; Freeman 2001; van de Ven et al. 2006). This high rotation and mass ($2.5 \pm 0.3 \times 10^6 M_{\odot}$, van de Ven et al. (2006)) gives the cluster a moderate ellipticity and a long relaxation time (Djorgovski 1993). An investigation into the global dynamics of the cluster can be found in van de Ven et al. (2006).

Perhaps most importantly, ω Cen is well known to display a complex stellar population, with a distinct metallicity spread among its stars (Dickens & Woolley 1967; Norris & Bessell 1975; Lee et al. 1999; Pancino et al. 2000; Sollima et al. 2005). This indicates that the cluster has undergone a star formation and chemical enrichment process that has been occurring over an extended period of time. Using helium abundances, Norris (2004) has shown that

the cluster has three distinct stellar populations, with corresponding metallicities ranging from -1.7 to -0.6 dex, with the majority of the stars (80%) belonging to the metal-poor branch. These values correspond to an age spread of around 2-3 Gyr. Furthermore, only the metal-poor populations ($[\text{Fe}/\text{H}] \leq -1.2$) seem to show evidence of rotation (Norris et al. 1997; Xie et al. 2002), although van de Ven et al. (2006) find no significant difference between the two populations. All observations suggest that the populations have different dynamical origins.

The origin of the cluster has been the subject of much debate, with the suggestion by several groups that it is the remnant of a dwarf galaxy disrupted by the Milky Way (Bekki & Freeman 2003; Iideta & Makino 2004). Indeed, Bekki & Norris (2005) postulate that the second generation population of ω Cen could have been formed from gas ejected from primordial stars which surrounded the cluster when it was once the nucleus of a dwarf galaxy.

The lack of observed mass segregation in the cluster (Anderson 1997; D'Souza & Rix 2005; Ferraro et al. 2006) may be further evidence that ω Cen was originally a more massive object. Based on the current mass of ω Cen and a distance of 5.5 Kpc, Ferraro et al. (2006) calculate a central relaxation time of ~ 6.6 Gyr, approximately a factor of two smaller than the cluster age, and thus expect there

to be some observable mass segregation in the cluster center. However, Ferraro et al. (2006) do not find any segregation in the cluster blue stragglers. They suggest two possible resolutions: that ω Cen was originally a much larger dwarf galaxy with a correspondingly larger relaxation time, and/or that the large rotation in ω Cen has increased the relaxation time, since angular momentum will keep stars out of the core. Further evidence of an external origin is that the cluster follows a highly bound retrograde orbit (Dinescu et al. 1999).

One way in which the cluster dynamical evolution can be studied is via variable stars, particularly eclipsing binaries. Detached binaries located at the cluster main sequence turnoff allow direct determination of the properties of turnoff stars in the cluster, important for the verification (or otherwise) of theoretical cluster isochrones. The detection of any new detached M-dwarf binaries also allows comparison with models of stellar evolution (Ribas et al. 2000). Binaries also provide calculations of stellar masses, radii, ages, luminosities (Giménez et al. 2001) and information on the evolution of both contact and detached systems. Hence, detection of new variable stars (particularly in the relatively understudied outer halo of the cluster) is useful for multiple scientific goals in furthering the understanding of the ω Cen stellar content.

Previous ground-based searches for cluster variable stars centered on the core have uncovered a rich population of many different types of variables, including SX Phe stars, eclipsing binaries (detached, semi-detached and contact systems), many RR Lyrae, spotted variables (variability associated with the rotational modulation of large starspots) and long period variables. The OGLE project has been the most prolific of these searches, with a total of 394 variables in their online catalogs (Kaluzny et al. 1996, 1997,b, 2004). Other deep variability searches have been more limited to the cluster core, for example Haggard et al. (2002).

The work presented here constitutes the results of a 25-night search for variability in a wide field centered on ω Cen which extends further from the cluster core and to deeper photometry than any previous ground-based variability survey. The search extends to $\sim 50\%$ of the cluster tidal radius (in a single exposure), corresponding to ~ 6.8 times the cluster half mass radius (Harris 1996). Hence the observed field contains a large majority of the bound cluster stars and has excellent prospects for the discovery of new variable systems, both in the cluster and the field.

The main motivation for the observations is to search for transiting ‘Hot Jupiter’ planets in the cluster, and is the second part of a search for such planets in both 47 Tucanae (Weldrake et al. 2005) and ω Cen. These two clusters are unique in that they display sufficient star brightness and total star numbers for meaningful statistics to be gained from a ground-based campaign with a telescope of moderate aperture. The results of the Hot Jupiter search in ω Cen will be published in a separate paper (Weldrake et al. 2006).

Section 2 of this work describes the observations and data reduction techniques employed to produce the total image dataset. Section 3 presents a description of the method used for time-series production and a discussion of the resultant photometric precision. Section 4 describes

the cluster Color-Magnitude dataset and astrometry, along with a description of the theoretical isochrones produced for the cluster. Section 5 details the methods used to detect the variable stars and section 6 presents the variable star catalog itself, with descriptions of the color-magnitude distribution of the variables, their spatial distributions and a discussion of the resulting catalog detection limits. Section 7 describes the analysis of individual variables (eclipsing binaries, RR Lyrae and miscellaneous pulsators), and Section 8 presents the paper summary and conclusions.

2. OBSERVATIONS AND DATA REDUCTION

The image dataset was obtained using the Australian National University (ANU) 40-inch (1m) telescope located at Siding Spring Observatory, fitted with the Wide Field Imager (WFI). This telescope and detector combination permits a $52' \times 52'$ (0.75 deg^2) field of view, capable of observing a large fraction of the cluster with a single exposure, thus maximising the number of sampled stars for lightcurve production. WFI consists of a 4×2 array of 2048×4096 pixel back-illuminated CCDs, arranged to produce a total array of $8K \times 8K$ pixels. The detector scale is $0''.38 \text{ pixel}^{-1}$ at the 1m telescope Cassegrain focus, allowing for suitable sampling of the point spread function (PSF) with the seeing limitations of the site. Our exposure times were fixed at 300 seconds resulting in excellent temporal resolution in the dataset.

The main aim of the project is the detection of ‘Hot Jupiter’ planet transits against ω Cen main sequence stars, which requires a signal-to-photon-noise ratio (S/N) of 200 or more for sufficient photometric precision ($\sim 1.5\%$) at $V=18.0$ (typical V magnitude of the target stars in these crowded fields). This requirement therefore defined the observing strategy. In order to achieve this with short exposure times, a broadband V+R filter was used, covering the combined wavelength range of the Cousins V and R filters. This same telescope and detector combination was used for a deep search for planet transits in the halo of 47 Tucanae, yielding a high significance null result (Weldrake et al. 2005). A total of 69 newly discovered variable stars were also found in that search (Weldrake et al. 2004). From this previous experience a star of $V=18.5$ in $2''$ seeing (typical of the site) yields a photon noise S/N of 220 with a 7-day moon and 165 at times of bright moon in a five minute exposure.

ω Cen was observed for a total of 25 contiguous nights, from 2003 May 2 to 2003 May 27 with the field centered at R.A = $13^h 26^m 45.89^s$, decl. = $-47^\circ 28' 36.7''$. The position of the centers of all CCDs can be found in Table 1. A total of 875 images of the cluster were obtained during this time, with an average temporal resolution of 6 minutes and covering an average 9 hours for each good night. Each image was independently checked at the telescope for cosmetic quality, and any with bad seeing ($> 3.5''$ images), satellite trails or other adverse effects were discarded from the dataset. Of this total database, 90% were deemed useful for the analysis, having suitable seeing and small telescope offsets to minimise star loss. A total of 787 images (with average seeing of $2.1''$) were subsequently used to produce 109,726 time-series via Differential Imaging Analysis (DIA, Wozniak (2000)) across the whole field for a detailed variability analysis.

Initial image reduction was performed according to standard practise within the MSCRED package of IRAF.¹ This incorporated region trimming, overscan correction, bias correction, flat-field and dark current subtraction. The images were then checked for flatness and overall quality and became available for the main photometric analysis and time-series production.

3. PHOTOMETRY AND PHOTOMETRIC ACCURACY

In order to obtain high precision photometry on relatively faint targets in the crowded field of a globular cluster, differential photometry was performed on the dataset. This method was originally described as an optimal Point-Spread-Function (PSF) matching algorithm by Alard & Lupton (1998), and was subsequently modified by Wozniak (2000) for use in detecting microlensing events. A detailed description of the method and software pipeline can be found in Wozniak's paper and only the main steps shall be summarized here.

The process of matching the stellar PSF throughout a large database of images dramatically reduces the systematic effects of varying atmospheric conditions on resultant photometric precision, allowing ground-based observations the best chance of detecting small brightness variations in faint targets. DIA is also one of the optimal photometric methods for dealing with crowded fields, as a larger number of pixels contain information on any PSF differences as the number of stars increases, hence improving the PSF matching process. Flux measurements of the stars are made via profile photometry on a master template frame, produced via the median-combining of a large number of the best quality images with small offsets. This template image is used as the zero-point in the output time-series.

The positions of the stars are found on a reference image, usually the image with the best seeing conditions, and all subsequent images in the dataset, including the template, are shifted to match. The best PSF-matching kernel is then found, and each registered image is subtracted from the template, with the residual subtraction generally being dominated by photon noise. Any object that has changed in brightness between the image and the template is given away as a bright or dark spot.

Differential photometry produces time-series measured in differential counts, a linear flux unit from which a constant reference flux (taken from the template) has been subtracted. In order to convert to a standard magnitude system, the total number of counts for each star was measured using the PSF photometry package of DAOPHOT within IRAF, with the same images and parameters as used in the photometry code. The time-series were then converted using these flux values into magnitude units via the relation:

$$\Delta m_i = -2.5 \log[(N_i + N_{\text{ref},i})/N_{\text{ref},i}]$$

where $N_{\text{ref},i}$ is the total flux of star i on the template image and N_i is the original difference flux in the time series as produced with the photometric code.

The pixel coordinates of all visible stars were determined separately from the reference frame via DAOFIND within

IRAF, and the profile photometry was then extracted from the subtracted frames at those determined positions. In this way, a total of 109,726 stars were identified and their time-series produced, across the whole WFI field, which then became the subject of analysis. The time-series are hence presented in this work in V+R differential magnitude units, and can be converted to the standard V system via the calculation of color terms. This requires another set of observations which is not directly related to the paper at hand.

3.1. Photometry of the cluster core

Each of the four outer CCDs of WFI were analysed in half CCD chunks, each half producing an average of 9,500 time-series. For the crowded core of the cluster, the number of stars becomes very large and, due to computational limitations, a different strategy was employed. For the core regions, the images were analysed individually with DIA in 360 individual subframes, 90 per CCD. The locations of these subframes were chosen so that no stars were lost at the edges of the subframes, covering the entire core region of the cluster, except those regions that were affected by telescope offsets during observing (a 160 pixel border surrounding each CCD).

Fig. 1 presents the resultant DIA-derived photometric precision, measured as root-mean-square scatter (rms), for a total of 104,381 stars which were cross-identified with the cluster CMD dataset. The left panel displays the rms of 60,123 stars within 13.5' of the cluster core and the right panel shows the rms of 44,258 stars outside this radius. The difference between these two crowding regimes is marginal, indicating the ability of DIA to handle fields of differing stellar density. The mean total star and background noise contribution is also plotted, illustrating that the photometry is photon-noise-limited to $V \sim 17.0$.

The position of the cluster main sequence turnoff (MSTO) is marked to indicate where the cluster stars become members of the main sequence. To the left of this line, therefore, lie likely Red Giant Branch and foreground Galactic disk stars. It can be seen that the photometric accuracy is equal to 2% (0.02 magnitudes) at $V \sim 18.5$ for both crowding regions of the data, increasing to 4% (0.04 magnitudes) at $V \sim 19.0$. By considering the stellar radius for cluster main sequence stars as a function of V , the photometry allows detection of transiting giant planets down to $V \sim 19.5$.

4. COLOR MAGNITUDE DIAGRAM AND ASTROMETRY

Using the same telescope/detector combination and pointing, a V, V-I color magnitude diagram (CMD) totalling 203,892 stars was produced for the observed field. This enabled detected variable stars and transiting systems to be placed on the standard V and I magnitude system, aiding in the determination of their likely nature. Three images in V and three in I were combined to produce the dataset, with all images being taken within 30 minutes to minimise the effect of variability on the resulting magnitudes and colors. Fig. 2 presents the diagram produced for all CCDs. The output DAOPHOT photometric errors in both V and V-I are marked as errorbars

¹ IRAF is distributed by National Optical Observatories, which is operated by the Association of Universities for Research in Astronomy, Inc., under cooperative agreement with the National Science Foundation.

as a function of V magnitude. The magnitude range of this diagram ($12.0 \leq V \leq 21.0$) covers a large range of stellar mass both in the cluster and the contaminating Galactic disk.

The CMD calibration was performed via matching of stellar astrometry from our catalog to that of Coleman (2004) (also taken with the ANU 1m and WFI combination in V and I), as standard field data were unavailable. The difference in V and I between our uncalibrated data and the Coleman (2004) calibrated data was measured for each of the matched stars (totalling more than 20,000) in each CCD independently; the resultant calibration accuracy was ≤ 0.03 magnitudes.

Also overplotted on Fig. 2 are three theoretical Yi et al. (2003) isochrones used to simulate the stellar populations of the cluster. These isochrones were used to determine stellar mass and radius values for cluster main sequence stars for use in the Hot Jupiter transit search. They also allow investigation into whether any particular type of variable is preferentially located within a particular population. The metallicity and relative fraction of each cluster population, as taken from Norris (2004), is also plotted.

Astrometry was obtained for a total of 212,959 stars identified in the V band image of the cluster, and 243,466 stars in the I -band. A search of the USNO CCD Astromograph Catalog (UCAC1) was carried out for astrometric standard stars within the field. Several hundred such stars were successfully identified, producing an accurate determination of the astrometric solution for the stars in each CCD, with measured uncertainties of $0.25''$.

In order to display the extent of our field of view with respect to the cluster, Fig. 3 presents both the total derived V band astrometric dataset (light shading) and the total time-series dataset (dark shading), plotted as ΔRA and ΔDec in degrees from the location of the cluster core. The eight CCDs of WFI are clear, as is the differing stellar densities encountered in the dataset. The time-series database (overplotted with darker shading) does not have the completeness of the total astrometry. The gaps are in regions where poor photometry resulted due to the presence of bright saturated stars or repeated measurements could not be obtained in a border surrounding each chip due to telescope offsets during the run. A total of 109,726 lightcurves were produced in the sampled regions.

Also overplotted on Fig. 3 as ellipses are the locations of the cluster core radius (innermost ellipse), the cluster half-mass radius (central ellipse) and the position of 50% of the cluster tidal radius (outer ellipse, the extent of the search). The ellipses have been plotted with the ω Cen ellipticity and cluster parameters of Harris (1996).

Fig. 4 shows the fraction of stars for which time-series information is available compared to the total astrometric database, as a function of radial distance from the cluster core. Our time-series database has an optimal region of $\sim 18'$ to $\sim 32'$ from the core. The decrease in completeness in the core and in the outer regions of the field are due to the gaps in the spatial coverage as seen in Fig. 3.

5. VARIABLE STAR DETECTION METHODS

In order to automatically detect the variable stars in the total time-series database, two search methods were used.

For any search, two main factors must be taken into account, namely the distribution of the observations in time and the shape of the variability for which the search is targeted. First, we applied the Lomb-Scargle Periodogram (LSP) (Bretthorst 2001) in which a Fourier power spectrum is produced with the same statistical properties as standard power spectra, but successfully overcomes the problems caused by diurnal gaps. The method produces a spike (with a frequency of $2\pi/P$) in the output power spectrum if a significant periodicity (P) is detected. The significance (in multiples of the standard deviation of the spectrum, σ) is determined for each datapoint independently.

If any datapoint is over a set detection threshold, a variable star candidate is flagged. By experimentation, it was found that for our dataset setting this detection threshold at $\geq 12 \times \sigma$ produces a variable star recoverability of 1 real variable per $\sim 1,000$ stars searched, with a corresponding false detection probability (per star) of 0.002%. In this manner, all stars in the time-series database were searched and the first sample of variable stars identified.

However, this method is only of benefit when searching for sinusoidal variability, and will miss detached systems and other non-sinusoidal stars. To overcome this, a second search was implemented on all stars using an application of the Analysis of Variance (AoV) statistic (O.Tamuz, private communication). A full description of this detection method can be found in Schwarzenberg-Czerny (1989). Via this method, the data are phase-wrapped with a trial period and then grouped into phase bins. A one-way statistical analysis of variance is then performed on the result. This statistical procedure is repeated for a fixed range of test periods for each star, producing a series of significances and their corresponding periodicities. The final output for each star is the peak periodicity and its corresponding significance.

Period estimates for the detected variables were derived by measuring the position of the highest significance peak in either the output power spectrum or the peak AoV statistic periodicity (in day units to 4 decimal places) and phase-wrapping the star at that period. The period was then tweaked manually to produce the smallest amount of scatter on the plotted lightcurve. The difference between the raw measured period and the final plotted period was smaller than 0.001 day in all cases, an indication of the accuracy of the detection methods.

6. VARIABLE STAR CATALOG OVERVIEW

As a result of analysing the whole dataset of 109,726 lightcurves, a total of 530 candidates were produced with a significant ($\geq 12\sigma$) periodicity as determined via LSP along with 2324 candidates with high significance ($\geq 8\sigma$) as determined with AoV. The AoV candidates include all of those detected via LSP. All candidates were then examined by eye both in their 'raw' un-phase-wrapped format and phase-wrapped to their peak detected periodicity. If the phase-wrapped lightcurve displayed discernable regular variability at the periodicities detected, they were flagged as variable stars. The vast majority of the candidates (particularly those identified by AoV) were found to be attributed to common systematic effects inherent to the data, associated with stars close to the magnitude limits

of the dataset.

In all, a total of 187 secure variable stars were identified, across the whole WFI field and are presented in Table. 2. The final catalog consists of 58 eclipsing binaries (EcB), 69 RR Lyrae stars, 36 Long Period Variables (LPVs, $P > 2d$) and 24 miscellaneous variables including 15 SX Phoenicis (δ Scuti) stars. From their locations on the cluster CMD, most of these systems are expected to be cluster members. Follow-up radial velocity observations are needed to confirm memberships. Of this sample, 81 of these variables are new discoveries as indicated by cross-matching astrometry with the Kaluzny et al. (2004) catalog. The time-series data are available on the electronic edition of AJ.

6.1. Comparison with Previous Studies

All of the detected variables were compared to the on-line catalog of Kaluzny et al. (2004) in order to identify new discoveries. A comparison was made of the published astrometry, period, type and V magnitudes of the known variables to the corresponding values derived in this work. We were able to match 106 of our variables with those of Kaluzny et al. (2004).

Fig. 5 shows the results of the comparisons made for these 106 recovered variables. The zeropoint was determined along with the standard deviation and has been overplotted for all parts of the figure for comparison. The comparisons are all consistent with zero. All matches within three arcseconds in both RA and DEC were classified as recovered variables, with the difference in derived astrometry both for RA and DEC seen in the top left panel of the figure. The final matching threshold was chosen by varying threshold, and comparing the number and period determinations of matches between the two datasets. Three arcseconds was found to produce the largest number of matches with the periods being consistent, a larger threshold introduces mis-matches. The average of the astrometry differences was found to be $0.005 \pm 0.005''$ for the RA astrometry and $0.232 \pm 0.233''$ for DEC. There is a slight systematic offset of $0.23''$ in declination between our catalog and that of Kaluzny et al. (2004). The sample of stars for which a large offset in astrometry is seen (num 40-60) is due to those variables being located in the most crowded regions of the cluster.

The top right panel shows the difference in derived period for these 106 stars. All recovered variables except six have periods presented here within 0.0005d of those published by Kaluzny et al. (2004), with an average very close to zero and standard deviation of 0.0002d. The remainder are all long period variables with a larger error in their period determination, due to incomplete phase coverage.

The bottom panel of Fig. 5 shows the difference in V magnitude as determined from our CMD dataset, and the average V magnitude as determined by Kaluzny et al. (2004). The plot shows some scatter around the zeropoint with an amplitude ~ 0.5 magnitudes, and has an average variation of -0.01 ± 0.42 mags. The range in V magnitude undertaken by the variable during the course of its variation is plotted as an errorbar for each point. Our measured V magnitude zero-point is within these errorbars for the vast majority of cases, indicating that the difference in V between our dataset and that of Kaluzny et al. (2004) (and

the subsequent 0.42 magnitude error) is caused by the various phases that each variable was undertaking when our CMD dataset was obtained.

A comparison in variable type was also made. For the 106 recovered variables, all but three have been assigned the same classification as in Kaluzny et al. (2004). These three (V42, V43 and V121) are classified as eclipsing binaries in this work, but were classed as RR Lyrae in Kaluzny et al. (2004). The time-series for these three can be seen in Fig. 10 and 13. For the cases of V42 and V121, the primary and secondary eclipses have a different depth (and shape), indicating their likeliness as an binary system. V43 seemingly displays secondary variations at times of maximum brightness, as seen in other binary lightcurves (ie, V13 and V178). Two of our variables were classified as unknown in the Kaluzny et al. (2004) catalog, and here are classified as an eclipsing binary (V84) and a long period variable (V104).

6.2. Color Magnitude Distribution

Fig. 6 shows the distribution of the variable stars overlaid on the Yi et al. (2003) theoretical stellar isochrones of ω Cen as determined with parameters taken from Norris (2004). Three isochrones were produced in total, each with the differing metallicities of the three distinct populations observed in ω Cen.

Eclipsing binaries are marked as blue triangles, RR Lyrae are plotted as green squares, the Long Period Variables are plotted as red hexagons, with the miscellaneous variables (δ Scuti's and other pulsators) marked as magenta pentagons. The eclipsing binary sample can be seen to follow the expected locations of blue straggler stars and binary main sequence members (located redward of the cluster main sequence). A few systems appear to lie on the cluster subgiant/red giant branch; if they are members, these stars are likely composed of at least one evolved component. Three systems seemingly lie on the cluster MSTO, although none are detached systems. These are hence less suitable than detached systems for determining the properties of turnoff stars in the cluster.

The RR Lyrae stars are seen to lie in the vast majority on the cluster HB instability strip, strongly implying their cluster membership. The other RR Lyrae lying off this sequence (those fainter and redder) we have classified as Galactic halo contamination (see Section 7.2). Many of the detected Long Period Variables (LPVs) appear to be associated with the cluster red giant branch, indicating their likely nature as evolved pulsators with cluster membership.

6.3. Spatial Distribution

The spatial distribution of the variable catalog, measured as the ΔRA and ΔDec in degrees for each variable from the core of the cluster, is presented in Fig. 7. Also marked as ellipses are the core radius (inner ellipse), the cluster half-mass-radius (middle ellipse) and 50% of the cluster tidal radius (outer ellipse, the limit of the search) produced with the same scale as Fig. 3. Each panel of Fig. 7 displays the distribution of a different type of variable.

Panel 'A' shows the distribution of the total catalog: those variables recovered from the catalog of Kaluzny et al. (2004) are marked as filled circles, new discoveries are

hence open circles. The new discoveries are located mainly in the outer regions of the field, due to the wide field employed in our search. The apparent gap in the distribution seen at $\Delta RA \sim 0.05$ is not real, but is due to the incompleteness of the lightcurve database at this location caused by telescope drift during observations. These limits to the regions where lightcurve production was impaired can be seen as the darker shading on Fig. 3. The vast majority of previously known variables that were not identified in our survey are either located in these parts of the dataset in the inner core of the cluster, a region to which this work is not sensitive. Panel ‘B’ displays the spatial distribution of the detected EcB stars. It can be seen that a slight majority (60%) are located towards the west of the cluster core. Panel ‘C’ shows the corresponding distribution of the detected RR Lyrae stars. These stars appear to be more centrally concentrated than the other types of variables, but this is due to incompleteness of fainter stars towards the cluster core, which truncates the frequency of the fainter EcB and LPV variables. As the EcB and LPV’s appear more homogeneously distributed over the cluster field, there do seem to be more EcB and LPV’s than RR Lyrae in the outer regions of the cluster. Panel ‘D’ is the distribution of the LPV stars.

6.4. Catalog Detection limits

Fig. 8 presents the total amplitude of each detected variable star plotted as a function of its corresponding V magnitude, in order to provide information on the detection limits of the catalog. Any variable star with an amplitude greater than or equal to the position of the dotted line is very likely to be detected in the dataset by the two detection methods described previously. Hence, at $V \sim 16.0$, this detection limit is about 0.015 magnitudes (1.5%), while at $V \sim 20.0$, the detection limit is 0.31 magnitudes (33%).

7. PRELIMINARY ANALYSIS OF INDIVIDUAL VARIABLES

Phase-wrapped differential V+R magnitude lightcurves of the detected variable stars are presented in Figs. 9 – 16 in order of discovery. Overplotted for each variable star is its identification number and determined period in days. The catalog as a whole is tabulated in Table 2. Those variables marked with ‘–’ in the last column of Table 2 are new discoveries.

7.1. Eclipsing Binaries

For the 58 EcB stars, it is clear that examples of contact (ie, V2), semi-detached (ie, V37) and detached (ie, V59) configurations are all present in the ω Cen field. These are classified considering the presence (or lack thereof) of features in the time-series indicating tidal distortion of the stellar components, the derived period, and the presence of any datapoints between individual eclipses, indicating physical separation of the stars. The majority (75%) are contact W-UMa-type systems, with apparent blue stragglers, binary main-sequence members and foreground variables identified from their locations on the cluster CMD (see Fig. 6). A further sample lie on the cluster Red Giant Branch (RGB), indicating that if they are cluster members they likely contain at least one evolved component.

Fig. 17 presents the radial distribution of EcB, measured as the distance in arcminutes from the position of

the core of the cluster. The light grey shaded histogram represents the radial distribution of the contact and semi-contact EcB (with periods ≤ 1 day), while the dark shaded histogram denotes the detached binaries. It can be seen that there is a marginal difference in the distribution of these two different types of binary systems; the results of a KS-test show that there is a 63% probability that they have the same distribution. In contrast, 47 Tucanae shows a clear segregation with contact binaries being preferentially located towards the cluster core with high significance (Weldrake et al. 2004). Also overplotted is the normalised total stellar distribution of the cluster (open histogram) and the theoretical King Profile (King 1962), as derived using the cluster parameters taken from Harris (1996). The total stellar distribution is seen to have a 100% completeness limit from $10'$ radius outwards.

The binary radial distribution shows an apparent gap in the population in the range $8' \rightarrow 15'$ from the cluster core. Other variable star types do not show this gap in their distributions, and so the effect is not thought to be attributed to variable star recoverability limits. From analysis via a KS test, there is only a 10% chance that the binaries are distributed in the same way as the other types of variable identified. This may be evidence for two populations of binary systems in the cluster and cannot be attributed to systematic dataset completeness limits. By compensating for the gaps in the time-series spatial coverage caused by telescope offsets during the observing run (hence regions where no time-series were produced), this binary distribution is enhanced rather than diminished.

This gap in binaries cannot be attributed to mass segregation as the cluster does not show any evidence of this (Anderson 1997; D’Souza & Rix 2005; Ferraro et al. 2006). It is possible that this distribution is related to the early life of the cluster as the nucleus of a dwarf galaxy (Bekki & Freeman 2003; Ideta & Makino 2004; Bekki & Norris 2005), which produced a base level of primordial binaries from gas-feeding, which we see as the outer population. Subsequent globular cluster processes (tidal and 3-body) would account for the increase in binarity towards the core. As the cluster relaxation time increases with radial distance due to longer interaction timescales, it is possible that the outer population is composed of the original primordial binaries (K.C.Freeman, private communication). The gap in the EcB distribution could indicate the boundary between these two effects, but it remains unclear with current data.

7.1.1. Peculiar Eclipsing Binaries

A number of binaries display interesting features in their lightcurves. Two systems have magnitudes and colors that place them on the cluster Horizontal Branch Instability Strip (hence in the same location as the RR Lyrae stars): V3 and V166. These could be systems that contain one pulsating component orbited by a secondary star (if members), or alternatively (perhaps more likely) they could be composed of one heavily distorted component with a small high-mass companion of foreground Galactic halo membership.

The first system, V3, has a short orbital period of 0.81 days and displays continuous sinusoidal variability with an eclipse of ~ 0.04 magnitudes depth. The eclipsing compan-

ion is strongly distorting the primary star. There seem to be two separate sequences of sinusoidal variability with the same period as the binary companion and an indication of an extended region of eclipse immediately before and after the main eclipse, perhaps indicating the presence of an accretion disk.

The second system of this same type, V166, is similar, displaying the same strong continuous sinusoidal variability with an eclipse (of ~ 0.16 magnitude depth), but with a longer orbital period of 2.06 days and much higher amplitude of variability. This star also shows the same two sequences of sinusoid, one sharp-edged and another more rounded with the same period as the binary companion. Both systems are worthy of future spectroscopic follow-up to determine their true nature.

A further binary system of note, V39, displays a single eclipse in the dataset with a total eclipse duration of ~ 3 days. Our data do not allow conclusions on the central shape of the eclipse. The color and magnitude of this system is consistent with a cluster member located high on the red giant branch, hence composed of at least one evolved giant star, consistent with an eclipse of long duration.

The derived period of this binary system, 34.8 days, has been determined by the appearance of secondary variations caused by tidal distortion of the primary star (even though only one eclipse was seen). The location of any secondary eclipse has been given away by the small-scale drop in brightness seen on these secondary variations. In this same way, other single eclipsers in the dataset have had their likely periods determined (ie, V71 and V161). These secondary-determined periods are denoted in Table 2 with a *, and the sinusoidal variability for these stars can be seen in their lightcurves in Figs. 9–16.

7.1.2. Low-Mass Eclipsing Binaries

Of the contact eclipsing binary sample, seven systems have orbital periods ≤ 0.25 days; V8, V10, V30, V68, V73, V80, and V124. Due to these very short periods, it is expected that these systems are composed of low-mass components, very likely late K to M dwarf stars. All of these systems have magnitudes and colors that overlay on the ω Cen binary main sequence, and hence most are likely members of ω Cen itself. Of this sample, V8, V10, V30 and V80 have V magnitudes in the range 19–21. The other stars are located approximately at the cluster turnoff.

Three detached binaries have orbital periods ≤ 1.6 days (V90, V102 and V153), with a further system with $P=2.46$ d (V41). These have been classified as detached systems due to the lack of observable secondary variations caused by the tidal distortion of the components occurring outside of the main eclipses and by the differing eclipse depths observed. These systems must be composed of low-mass components (perhaps both in the M-dwarf regime) for them to display such short periods without the effects of tidal distortion on the lightcurves. The identification (and confirmation) of M-dwarf detached binaries is of great importance in the production of stellar evolutionary models since they allow determination of masses and radii towards the low end of the mass function for comparison to theoretical predictions.

Of particular interest is V153, a detached binary with

an orbital period of 0.83 days. The color and magnitude of this star place it blueward of the blue-straggler branch of the CMD, and hence in an unusual place for a detached binary member of the cluster (which should lie on one of the main CMD sequences). In fact, the V-I value of 0.19 is unusually blue for a detached binary of such short period, which would ordinarily be composed of red components. From our observations of the period and color, considering the distinct observed eclipses (with somewhat flat bottoms) and lack of any observable tidal distortion, we conclude that this binary is very likely a foreground system, with an uncertain composition, perhaps containing a pair of white dwarf stars. Such a system would be a prime candidate for future spectroscopic observations to determine its true nature.

7.2. RR Lyrae

A total of 69 RR Lyrae stars were identified in the dataset, the vast majority of which are likely members of the cluster, due to their firm location on the cluster Horizontal Branch. Of the total sample, 59% are examples of RR Lyrae type ‘AB’ (fundamental mode pulsators) and 41% are examples of the shorter period RR Lyrae type ‘C’ (first harmonic mode pulsators) based on the shape of their phase-wrapped lightcurves and periods. Type ‘C’ stars are typically less common than Type ‘AB’ (Vivas et al. 2001). None of the rare longer period RR Lyrae AHB1 stars (Sandage, Diethelm, & Tammann 1994) were seen in our data. Twenty-six of our RR Lyrae are new discoveries.

Fig. 18 shows the period distribution (left panel) and the period-luminosity diagram (right panel) for our RR Lyrae sample. The period distribution displays two distinct populations, one peaking at pulsation period ~ 0.35 days and the other at period ~ 0.65 days. These constitute the RR Lyrae type ‘C’ and type ‘AB’, respectively. Fig. 19 shows the period versus V+R amplitude plot for our sample of RR Lyrae stars.

The period-luminosity diagram shows that the majority of RR Lyrae (of both types) are clustered around $V\sim 14.5$ and are hence likely ω Cen members. A small number of the sample are significantly fainter, running from $V\sim 15.0\rightarrow 19.5$. The outliers are attributed to background contamination by the Galactic Halo. Our photometry becomes saturated at $V\sim 14.0$ (as seen in Fig. 1) and hence there are no foreground RR Lyrae detected in the dataset with brighter V magnitudes than this.

To determine memberships based on the magnitude distribution, an application of KMM mixture modelling (Ashman et al. 1994) was applied, which assumes gaussian distributions with differing dispersions. As a first check, the faintest six RR Lyrae were removed using 3-sigma clipping, producing a mean V magnitude of 14.50 ± 0.33 for the remaining 63 stars. In comparison, KMM modelling was applied to the total sample with two gaussians, which produced two samples, one with the 62 brightest RR Lyrae and another with the remaining 7 fainter stars. The result is that everything brighter than and including $V=15.245$ (62 stars) is considered a cluster member based on its brightness. The mean of these 62 (for both AB and C type RR Lyrae) is 14.51 ± 0.04 , with the error being the standard deviation of the mean, seen overplotted in the right panel of Fig. 18.

From our total RR Lyrae sample, it is possible to calculate the distance modulus of the cluster. It is well known that the absolute magnitude of RR Lyrae stars is dependent on metallicity (Sandage 1981a,b), and from studies of RR Lyrae and horizontal branch stars in the Milky Way, the LMC and M31 clusters this relation has been recently adopted with a slope in the range 0.20-0.23 mag/dex (Clementini et al. 2003; Cacciari & Clementini 2003; Gratton et al. 2004). Rich et al. (2005) have adopted a relation of the form $M_V = 0.20 \pm 0.09 [\text{Fe}/\text{H}] + 0.81 \pm 0.13$, which is also used in this work.

Several of our RR Lyrae sample could be crossidentified with the sample of Rey et al. (2000), which have metallicity measurements associated with them. Fig. 20 shows the $[\text{Fe}/\text{H}]$ distribution for the 53 of our RR Lyrae sample, which were crossidentified with these Rey et al. (2000) metallicity estimates. Two Gaussians were fitted via least squares to describe this distribution. The resulting Gaussians are overplotted in Fig. 20, with their peak $[\text{Fe}/\text{H}]$ and relative fractions noted. From the area under the gaussian fits, 82% of the sample belong to a population with $[\text{Fe}/\text{H}] = -1.71$ with the remaining 18% belonging to a $[\text{Fe}/\text{H}] = -1.25$ population. The dispersions of these two Gaussians are measured as 0.20 and 0.07 dex respectively, being composed of the natural dispersion of the sample and the uncertainty in the $[\text{Fe}/\text{H}]$ measurements as presented by Rey et al. (2000). We assume that the remaining 16 RR Lyrae in our sample with unknown $[\text{Fe}/\text{H}]$ follow these same relative distributions.

The absolute magnitude (M) of the most metal poor population is 0.47 ± 0.28 as determined via the Rich et al. (2005) relationship, with $M = 0.56 \pm 0.24$ for the second more metal rich group. By considering the relative fractions of the sample in each population, the weighted mean absolute magnitude estimated for our total RR Lyrae sample is 0.48 ± 0.27 .

The mean V apparent magnitude for the cluster RR Lyrae sample (of all metallicities) is 14.51 ± 0.04 with the error being the standard deviation of the mean. This leads to an apparent distance modulus of 14.04 ± 0.27 (6.4 ± 0.7 kpc). This compares well to the Harris (1996) value of 13.97 and the Kaluzny et al. (2002) estimate of 14.09 ± 0.04 as derived from an eclipsing binary star. Our apparent value is around 0.3 magnitudes brighter than that of van de Ven et al. (2006), who find a best-fit dynamical distance modulus of 13.75 ± 0.13 . The cluster has a non-zero reddening, and if we apply the $E(B-V) = 0.12$ value of Harris (1996), we arrive at a reddening-corrected distance modulus of 13.68 ± 0.27 (5.4 ± 0.7 Kpc). This compares well to the reddening-corrected estimate of 13.70 ± 0.06 from (Del Principe et al. 2006).

A small number of the RR Lyrae appear to display small-scale secondary variations in the general shape of the lightcurve and are examples of Blazhko RR Lyrae (Blazhko 1907). Examples of this effect are seen in V48, V105, V110, V111, V128, V136, V173 and V183. Quite significant variations are seen particularly in V111, V128 and V183. Such variations are a little understood feature of some RR Lyrae, and are generally thought to be caused by strong photospheric magnetic fields (Cousens 1983) and/or rotation (Dziembowski & Cassisi 1999). The effect is dependent on the metallicity of the star (Alcock

et al. 2003) and is found preferentially in association with type ‘AB’ RR Lyrae. We note, however, that V183 cannot be easily phase-wrapped and seems to be undergoing a period change. Due to their sinusoidal lightcurves, their faintness compared to the cluster HB and small amplitude, it is possible that V53, V99 and V155 are eclipsing binary stars, and are classified as either RR Lyrae or EcB in Table. 1. As only a small fraction of the lightcurve for V146 was observed, the derived period in Table 1 is uncertain, but due to its location on the cluster CMD it has been classified here as an RR Lyrae. Further photometry is needed to fully determine its type.

7.3. Long Period Variables and Miscellaneous Variables

In this work, an LPV is defined as having a pulsation-like lightcurve with a periodicity ≥ 2 days. Compared to some types of variables (ie, Mira-type stars), the LPVs found in this dataset have very short periods. The length of our observing window (25 nights) and saturation limit precludes the detection of variable stars with excessively long pulsation periods (\sim years), which would exist in the bright AGB region of the cluster population. Despite this, a rich sample of LPVs with relatively short pulsation periods have been detected in the dataset.

From their locations in Fig. 6, approximately 75% of the detected LPVs are expected to be members of the cluster. A small number (~ 6) seem to lie on the cluster main sequence. The rest seem too red and faint to be consistent with the cluster stellar populations. Of particular interest are V98 ($P = 21.8$ days) and V125 ($P = 4.8$ days). The lightcurves for these two stars appear to show eclipses superimposed on the pulsation, which we are able to discern due to the high temporal resolution of the data. Both are likely cluster members.

The miscellaneous variables are comprised of 15 SX Phoenicis (δ Scuti) stars and nine other pulsators of various types. The SX Phe are, in the majority, in the cluster blue-straggler region and hence these are regarded as likely cluster members. All have very short periods, typical of the class, with the shortest being ~ 0.038 days. Two other pulsators, V164 and V109 have been classified as Type-II Cepheids (Nemec et al. 1994). V19 could be a binary system or a pulsator. Finally, we classify V1, V4, V15 and V50 and V74 as regular short period pulsators of uncertain type.

8. SUMMARY AND CONCLUSIONS

We have presented the V+R lightcurves and a preliminary analysis of 187 variable stars detected in a $52' \times 52'$ field centered on the globular cluster ω Cen, as part of an extensive search for transiting ‘Hot Jupiter’ planets in the cluster, which will be presented elsewhere. Of the variables presented here, 81 are new discoveries. The catalog in total comprises 58 eclipsing binaries, including contact, semi-detached and detached configurations; 69 RR Lyrae stars, 36 Long Period Variables, and 24 miscellaneous variables including 15 SX Phe stars and two TypeII Cepheids. From their locations on the cluster Color Magnitude Diagram, the majority of our detected variables are consistent with having cluster memberships.

The eclipsing binary radial distribution displays an apparent lack of binaries (of both contact and detached

types) in the $8' \rightarrow 15'$ range, perhaps indicating the presence of two separate binary populations. This trend cannot be attributed to completeness limitations in the dataset. The origin of the spatial gap in the binaries is unclear.

Of the total binary sample, four detached systems have short orbital periods. When combined with their observed V-I colors, three are consistent with being composed of M-dwarf stars, important for comparisons with stellar evolution models. One further detached system has an orbital period of only 0.8 days and, given its blueness, may be composed of white dwarf stars. Another eclipsing system has a single observed eclipse with a duration of ~ 3 days, due to the presence of one evolved component. We deduce a reddening corrected distance modulus of 13.68 ± 0.27 for the cluster, based on the RR Lyrae in our sample.

We also present an extensive V and I photometric database (with astrometry better than $0.25''$) for 203,892 stars in our 0.75 deg^2 field of view centered on the cluster, and V+R lightcurves spanning 25 nights for 109,726 stars ($14.0 \leq V \leq 22.0$) for both the cluster and the field.

ACKNOWLEDGMENTS

The authors would like to thank the following people for their contributions in the production of this work: Omer Tamuz for many discussions on the merits of the AoV detection method; Laura Stanford for help with the production of the theoretical isochrones; John Norris and Ken Freeman for discussions on the binary radial distribution; and Cristina Afonso for helpful information about KS tests. We also thank Gisella Clementini for acting as a very thorough and helpful referee.

REFERENCES

- Alard, C. & Lupton, R. H. 1998, *ApJ*, 503, 325
 Alcock, C., et al. 2003, *ApJ*, 598, 597
 Anderson, A. J. 1997, Ph.D. Thesis, Univ. of California Berkeley
 Ashman, K. M., Bird, C. M., & Zepf, S. E. 1994, *AJ*, 108, 2348
 Bekki, K., & Freeman, K. C. 2003, *MNRAS*, 346, L11
 Bekki, K., & Norris, J. E. 2005, *ApJ*, submitted, astro-ph/0512385
 Blazhko, S. 1907, *Astron. Nachr.*, 175, 325
 Bretthorst, G. L. 2001, *AIP Conf. Proc.* 568: Bayesian Inference and Maximum Entropy Methods in Science and Engineering, 568, 241
 Cacciari, C., & Clementini, G. 2003, *LNP Vol. 635: Stellar Candles for the Extragalactic Distance Scale*, 635, 105
 Clementini, G., Gratton, R., Bragaglia, A., Carretta, E., Di Fabrizio, L., & Maio, M. 2003, *AJ*, 125, 1309
 Coleman, M. G. 2004, Ph.D. Thesis, Australian National University
 Cousins, A. 1983, *MNRAS*, 203, 1171
 Dickens, R. J., & Woolley, R. v. d. R. 1967, *Royal Greenwich Observatory Bulletin*, 128, 255
 Dinescu, D. I., Girard, T. M., & van Altena, W. F. 1999, *AJ*, 117, 1792
 Djorgovski, S. 1993, *ASP Conf. Ser.* 50: Structure and Dynamics of Globular Clusters, 50, 373
 Del Principe, M. et al. 2006 astro-ph/0608052
 D.Souza,R., & Rix,H.R. 2005, astro-ph/0503299
 Dziembowski, W. A. & Cassisi, S. 1999, *Acta Astronomica*, 49, 371
 Ferraro, F. R., Sollima, A., Rood, R. T., Origlia, L., Pancino, E., & Bellazzini, M. 2006, *ApJ*, 638, 433
 Freeman, K. C. 2001, *ASP Conf. Ser.* 228: Dynamics of Star Clusters and the Milky Way, 228, 43
 Giménez, A., Ribas, I., & Guinan, E. F. 2001, *ASP Conf. Ser.* 245: Astrophysical Ages and Times Scales, 245, 301
 Gratton, R. G., Bragaglia, A., Clementini, G., Carretta, E., Di Fabrizio, L., Maio, M., & Taribello, E. 2004, *A&A*, 421, 937
 Haggard, D., Carlin, J. L., Cool, A. M., Zhao, B., Bailyn, C. D., Edmonds, P. D., Grindlay, J. E., & Davies, M. B. 2002, *Bulletin of the American Astronomical Society*, 34, 654
 Harris, W. E. 1996, *AJ*, 112, 1487
 Ideta, M., & Makino, J. 2004, *ApJ*, 616, L107
 Kaluzny, J., Olech, A., Thompson, I. B., Pych, W., Krzeminski, W., & Schwarzenberg-Czerny, A. 2004, *VizieR Online Data Catalog*, 342, 41101
 Kaluzny, J., Kubiak, M., Szymanski, M., Udalski, A., Krzeminski, W., & Mateo, M. 1996, *A&AS*, 120, 139
 Kaluzny, J., Kubiak, M., Szymanski, M., Udalski, A., Krzeminski, W., & Mateo, M. 1997, *A&AS*, 125, 343
 Kaluzny, J., Kubiak, M., Szymanski, M., Udalski, A., Krzeminski, W., Mateo, M., & Stanek, K. 1997, *A&AS*, 122, 471
 Kaluzny, J., Thompson, I., Krzeminski, W., Olech, A., Pych, W., & Mochejska, B. 2002, *ASP Conf. Ser.* 265: Omega Centauri, A Unique Window into Astrophysics, 265, 155
 King, I. 1962, *AJ*, 67, 471
 Lee, Y.-W., Joo, J.-M., Sohn, Y.-J., Rey, S.-C., Lee, H.-C., & Walker, A. R. 1999, *Nature*, 402, 55
 Merritt, D., Meylan, G., & Mayor, M. 1997, *AJ*, 114, 1074
 Meylan, G., & Mayor, M. 1986, *A&A*, 166, 122
 Nemec, J. M., Nemec, A. F. L., & Lutz, T. E. 1994, *AJ*, 108, 222
 Norris, J., & Bessell, M. S. 1975, *ApJ*, 201, L75
 Norris, J. E., Freeman, K. C., Mayor, M., & Seitzer, P. 1997, *ApJ*, 487, L187
 Norris, J. E. 2004, *ApJ*, 612, L25
 Olech, A., Kaluzny, J., Thompson, I. B., & Schwarzenberg-Czerny, A. 2003, *MNRAS*, 345, 86
 Pancino, E., Ferraro, F. R., Bellazzini, M., Piotto, G., & Zoccali, M. 2000, *ApJ*, 534, L83
 Rey, S.-C., Lee, Y.-W., Joo, J.-M., Walker, A., & Baird, S. 2000, *AJ*, 119, 1824
 Ribas, I., Jordi, C., & Giménez, Á. 2000, *NATO ASIC Proc.* 544: Variable Stars as Essential Astrophysical Tools, 659
 Rich, R. M., Corsi, C. E., Cacciari, C., Federici, L., Fusi Pecci, F., Djorgovski, S. G., & Freedman, W. L. 2005, *AJ*, 129, 2670
 Sandage, A. 1981, *ApJ*, 244, L23
 Sandage, A. 1981, *ApJ*, 248, 161
 Sandage, A., Diethelm, R., & Tammann, G. A. 1994, *A&A*, 283, 111
 Schwarzenberg-Czerny, A. 1989, *MNRAS*, 241, 153
 Sollima, A., Ferraro, F. R., Pancino, E., & Bellazzini, M. 2005, *MNRAS*, 357, 265
 van de Ven, G., van den Bosch, R. C. E., Verolme, E. K., & de Zeeuw, P. T. 2006, *A&A*, 445, 513
 Vivas, A. K., et al. 2001, *ApJ*, 554, L33
 Weldrake, D. T. F., Sackett, P. D., Bridges, T. J. 2006, in prep
 Weldrake, D. T. F., Sackett, P. D., Bridges, T. J., & Freeman, K. C. 2005, *ApJ*, 620, 1043
 Weldrake, D. T. F., Sackett, P. D., Bridges, T. J., & Freeman, K. C. 2004, *AJ*, 128, 736
 Wozniak, P. R. 2000, *Acta Astronomica*, 50, 421
 Xie, B., Pryor, C., Hilker, M., Gebhardt, K., & Williams, T. B. 2002, *Bulletin of the American Astronomical Society*, 201, 706
 Yan, L. & Reid, I. N. 1996, *MNRAS*, 279, 751
 Yan, L. & Mateo, M. 1994, *AJ*, 108, 1810
 Yi, S. K., Kim, Y.-C., & Demarque, P. 2003, *ApJS*, 144, 259

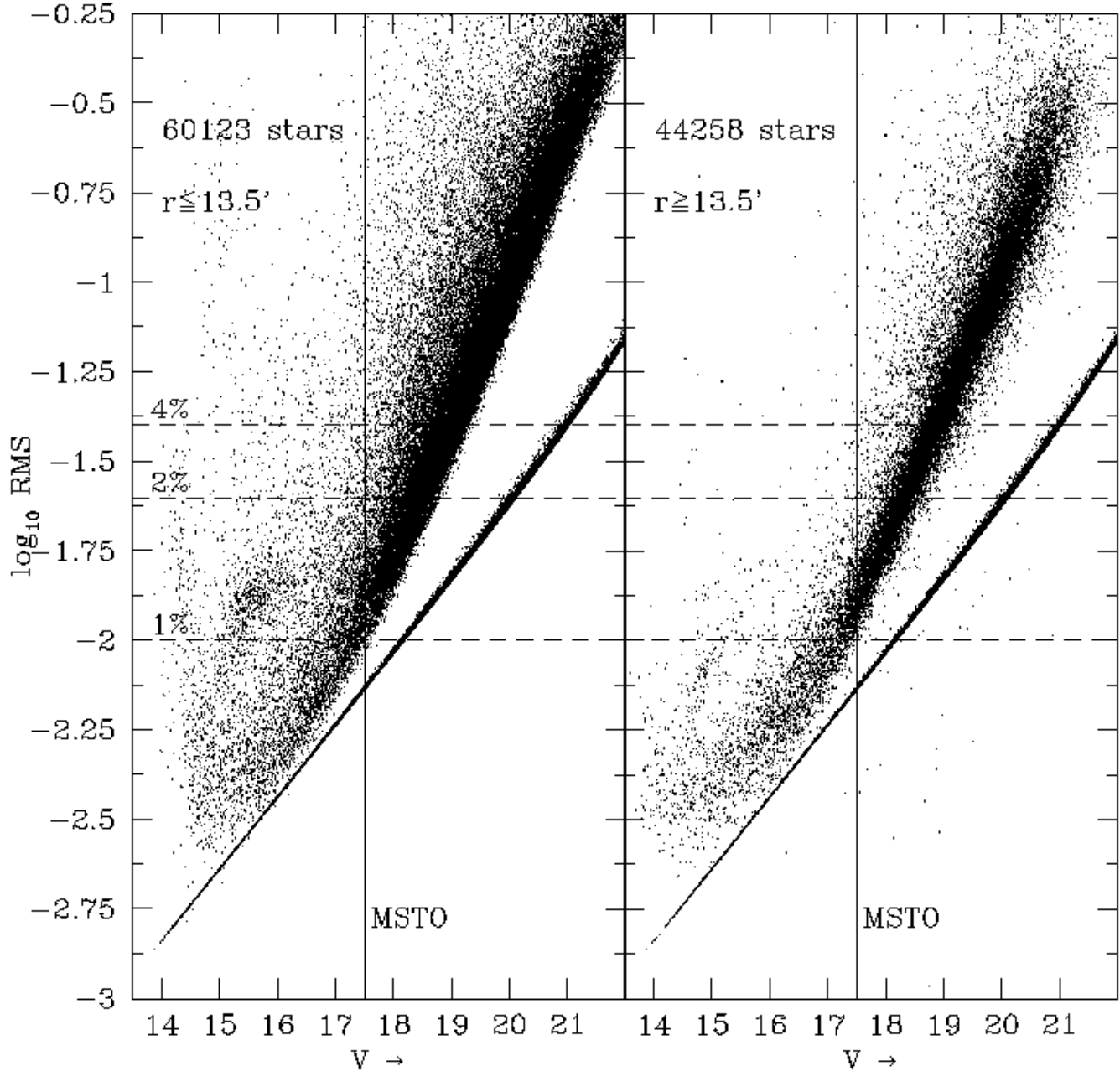


FIG. 1.— The measured DIA photometric scatter for a total of 104,381 stars which were cross-identified with the CMD dataset. The mean total star+background photon noise contribution is also indicated for each star (thin locus of points). Those stars located within and outside 13.5' of the cluster core are plotted separately; the difference in photometric precision between these two crowding regimes is marginal. The position of the cluster main sequence turnoff (MSTO) is marked to indicate photometric rms for cluster main sequence stars. The uncertainty is 1% at the MSTO and 4% (0.04 mag) at $V \sim 19.0$.

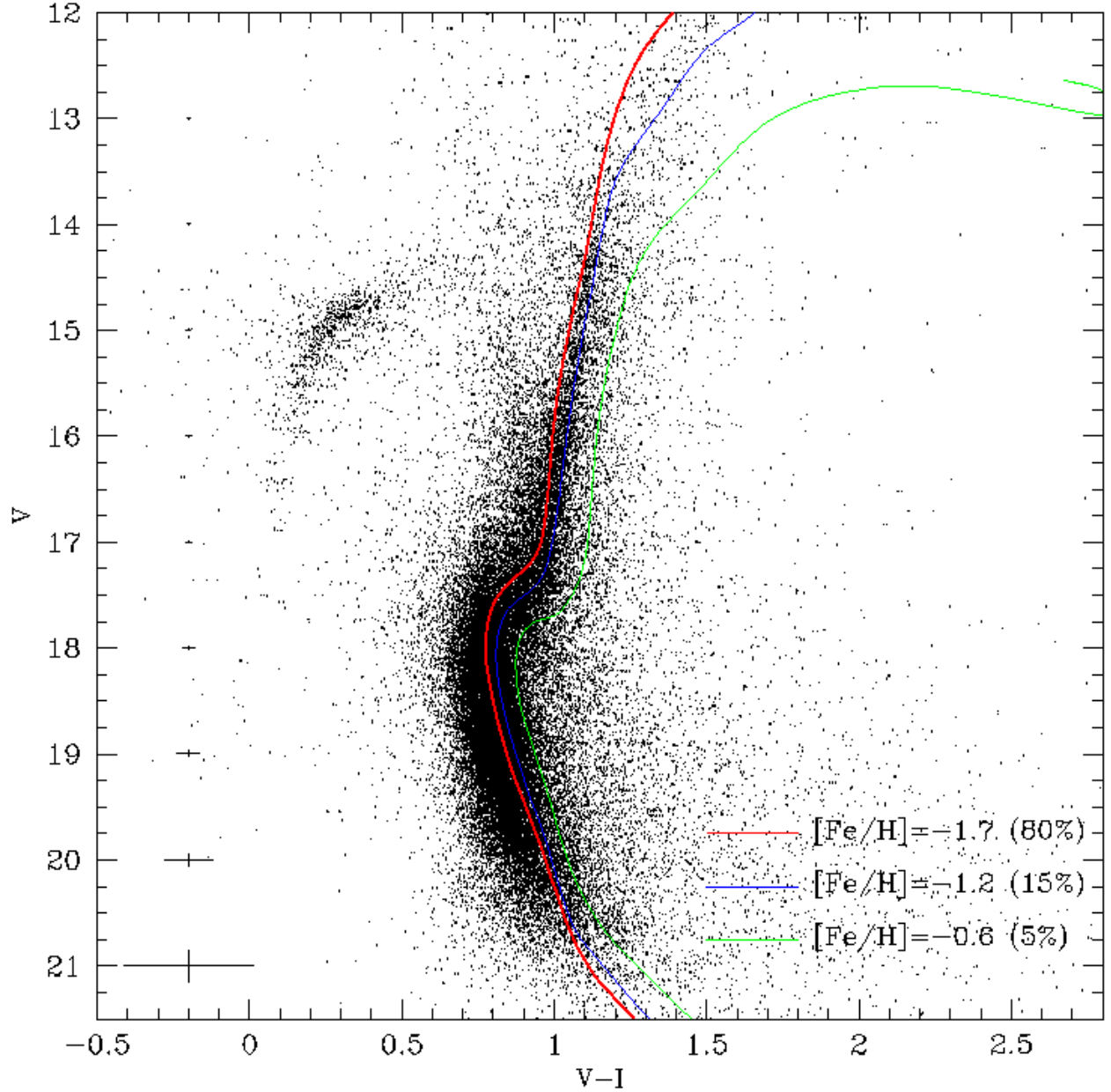


FIG. 2.— The Color Magnitude Diagram (CMD) dataset used to derive color information for variable objects. The DAOPHOT output errors are marked as errorbars as a function of V . Also overplotted are the three theoretical Yi et al. (2003) isochrones to define the stellar populations of the cluster. The metallicity and relative fraction of each isochrone as taken from Norris (2004) is marked accordingly. The CMD calibration is accurate to better than 0.03 mag as described in the text.

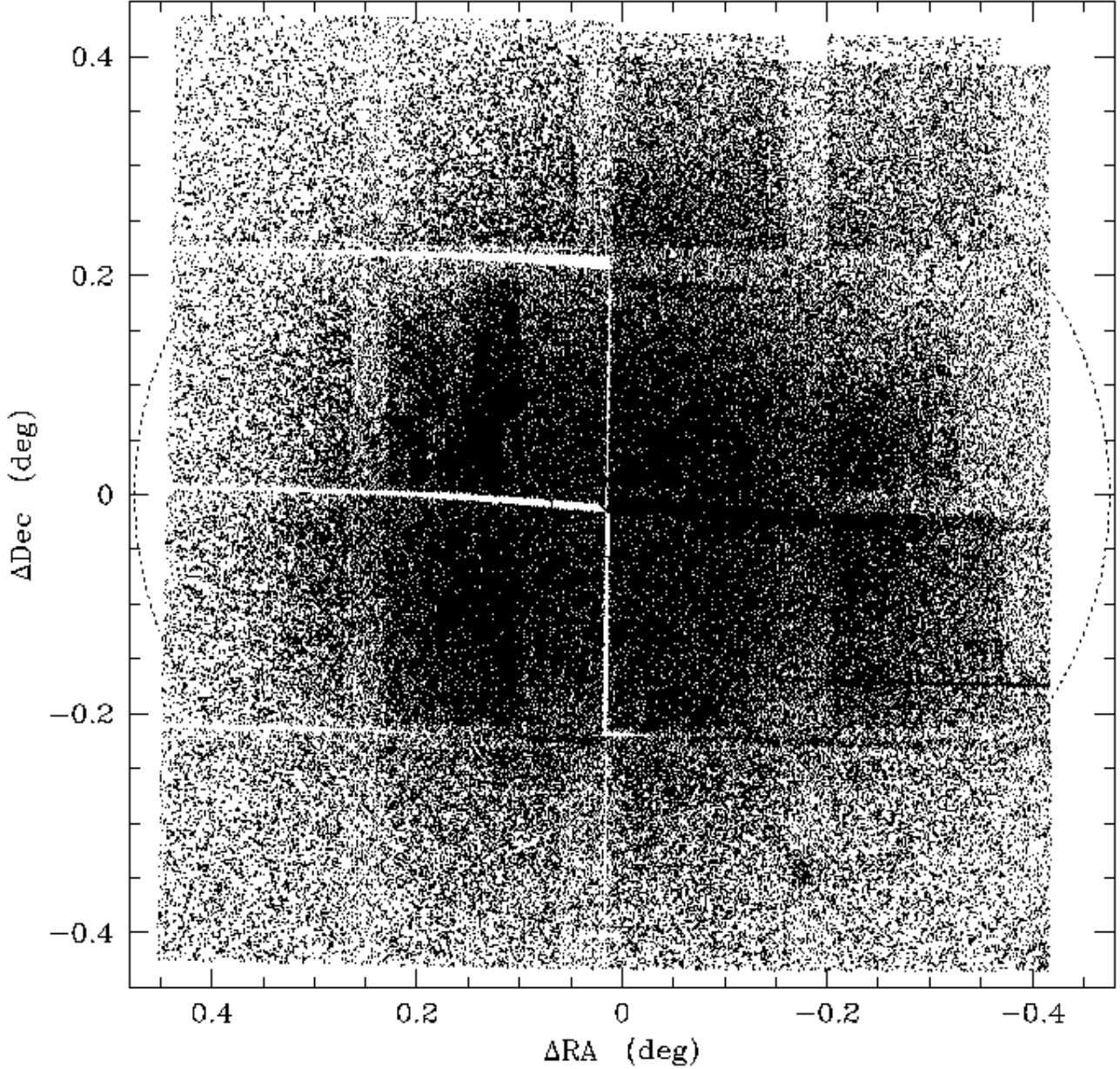


FIG. 3.— The total derived V band astrometry (light shading) plotted as ΔRA and ΔDec (in degrees) from the location of the cluster core for 212,957 stars. The extent of the eight WFI CCDs are clear, as well as the differing stellar densities encountered in the dataset. Also overplotted (darker shading) are the locations of stars for which time-series production was possible. The gaps in the spatial coverage are caused by the spaces separating CCDs and regions where stellar density (and saturation) did not allow sufficient accuracy in the output DIA templates and subtracted frames or by telescope offsets. We have time-series information for 54% of the stars for which we have astrometry. The three ellipses (plotted with the ω Cen ellipticity and cluster parameters taken from Harris (1996)) define the positions of the cluster core radius (inner ellipse), the cluster half-mass radius (central ellipse) and the position of 50% of the cluster tidal radius (outer ellipse) - the extent of our single WFI field of view.

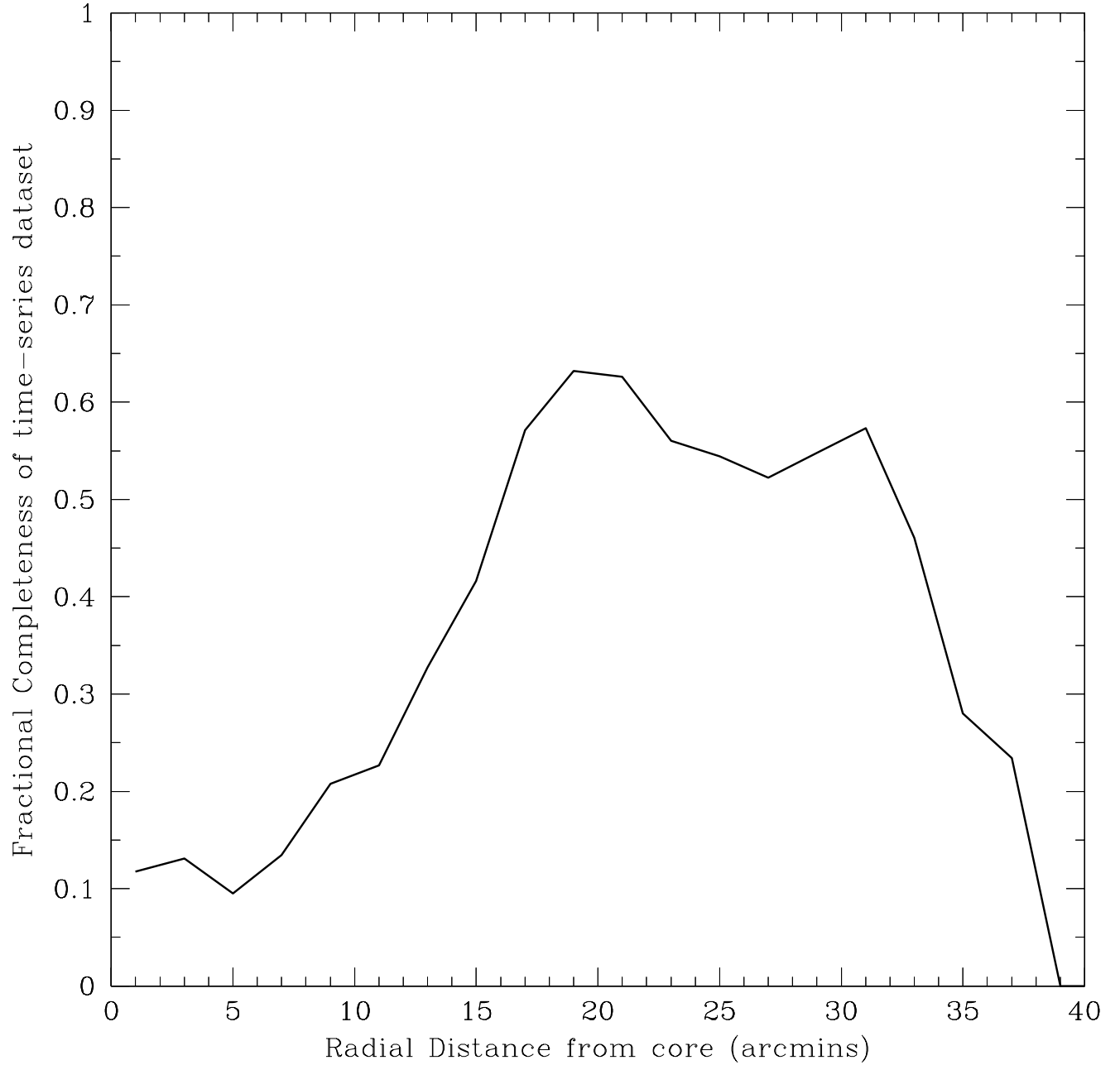


FIG. 4.— The fraction of stars with time-series information compared to the total astrometric stellar database, as a function of radial distance from the cluster core. The truncation in fraction is caused by the gaps in spacial coverage of the cluster, as seen in Fig. 3. The time-series dataset has an optimal zone from $\sim 18'$ to $32'$ from the cluster core.

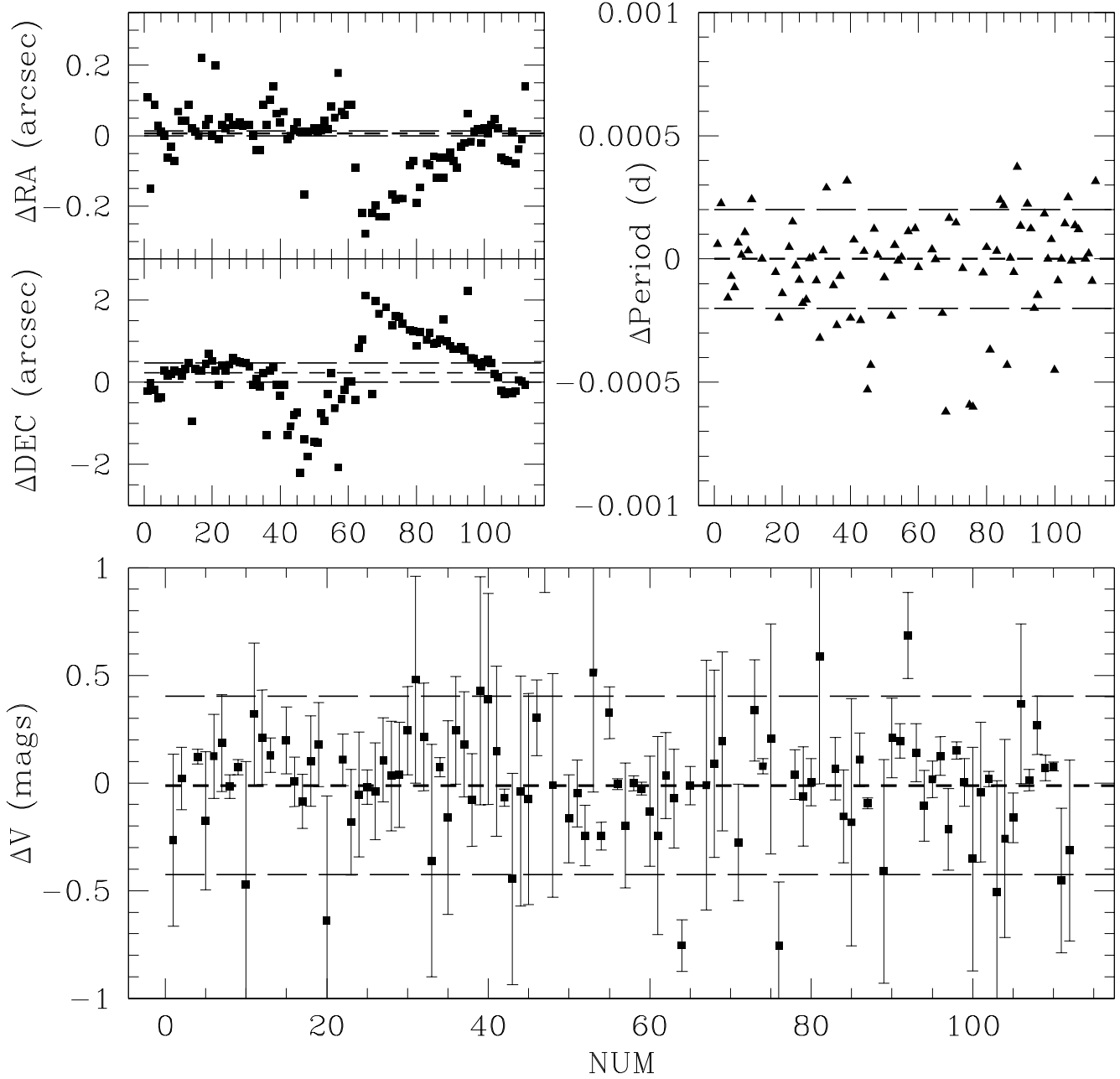


FIG. 5.— A comparison of previously known variables from the Kaluzny et al. (2004) online database, with an arbitrary identification number on the X-axis. Plotted are the differences in astrometry (top left panel), the differences in derived period (top right panel) and the differences in measured V magnitude (bottom panel). The zero-point for all panels has been overplotted for comparison. The difference in the astrometry for those crossidentified variables is less than $\text{RA}=0.3''$ and $\text{DEC}=3''$ for all cases and the derived periods are seemingly accurate between the two datasets to $P\sim 0.0005$. The V magnitude values presented in this work are measured directly from the CMD dataset, and have a subsequent scatter of ~ 0.4 magnitudes when compared to the average V magnitudes of Kaluzny et al. (2004). The errorbars denote the range in V magnitude the variable undergoes. Our V magnitudes are within these errorbars for the majority of cases.

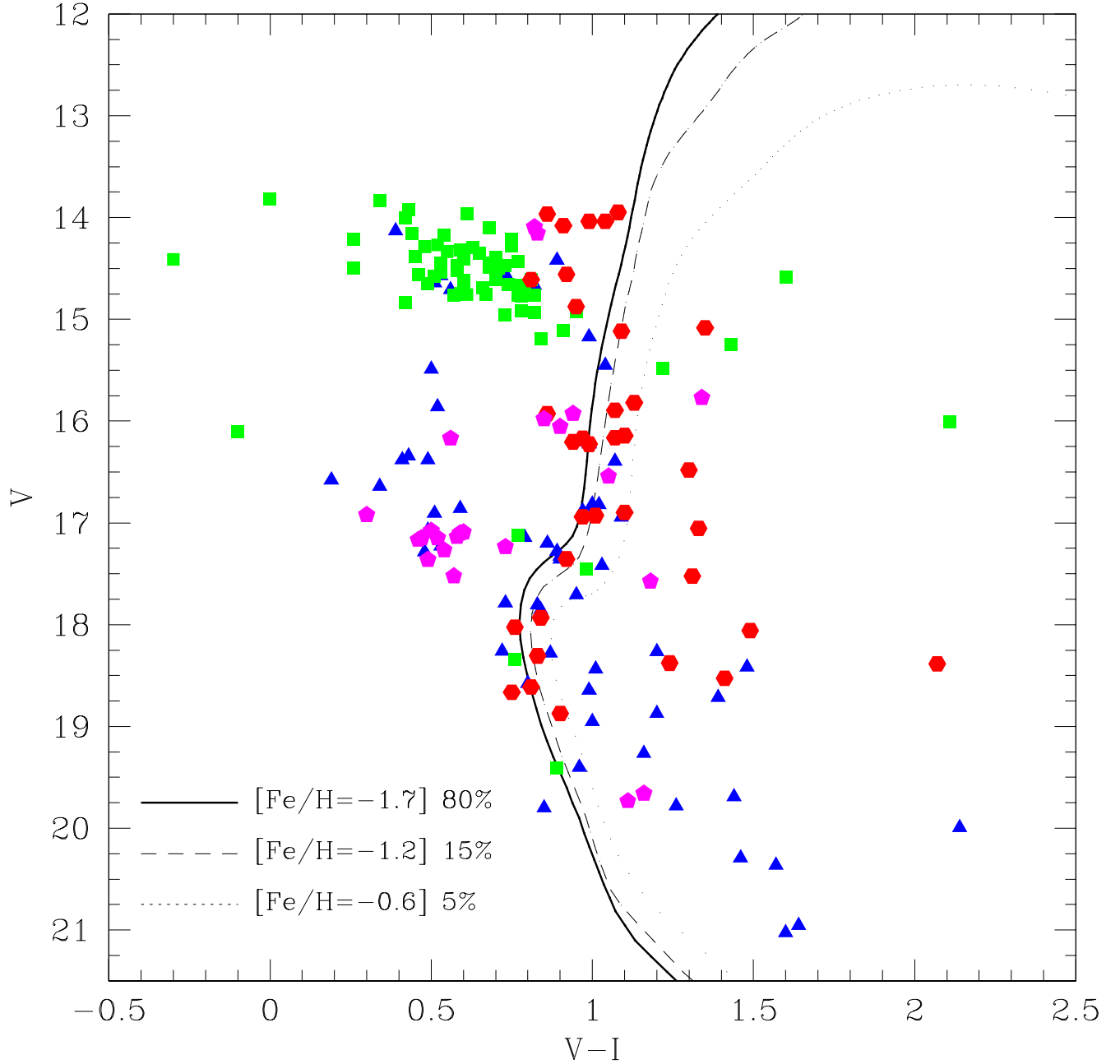


FIG. 6.— The theoretical CMD for ω Cen, calculated using Y2 isochrones (Yi et al. 2003), with our detected variable stars overplotted. Three isochrones are plotted, with metallicity values taken from (Norris 2004) to describe the total stellar population of the cluster. The fraction of stars that belong to each isochrone is also marked. Eclipsing binaries (EcB) are plotted as blue triangles, RR Lyrae as green squares, long period variables (LPVs) as red hexagons. The other miscellaneous variables (SX Phe stars and other pulsators) are marked as magenta pentagons. Clearly, different populations of variable stars are seen in the dataset. The EcB run from the blue straggler regime (where also most of the SX Phe stars lie) and follow the binary main sequence. Hence the majority are expected to be members of the cluster. The RR Lyrae stars are located within the Horizontal Branch instability strip and most are expected to be cluster members. The LPV stars appear to be positioned on the cluster red giant branch with some foreground variables.

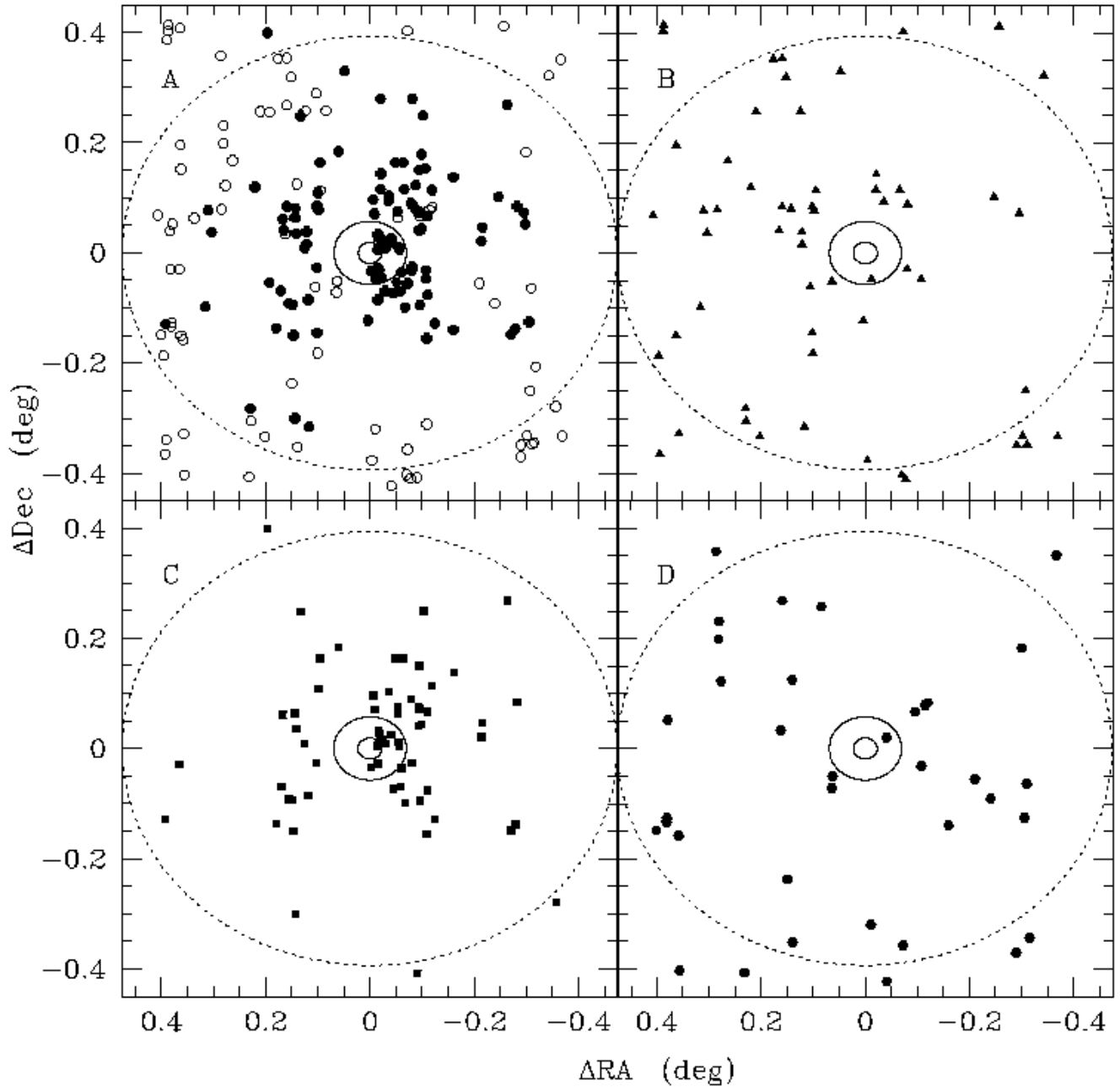


FIG. 7.— The spatial distribution of the detected variable stars, measured as ΔRA and ΔDec (in degrees) from the core of ω Cen. The plots have been made to the same scale as in Fig. 3. The two inner ellipses correspond to the core and half mass radii of the cluster, and the large outer ellipse defines 50% of the cluster tidal radius, indicating the extent of the dataset. Panel 'A' displays all variable stars, with new discoveries marked as open circles. Panel 'B' shows the distribution of eclipsing binaries, panel 'C' the RR Lyrae stars, and panel 'D' the long period variables.

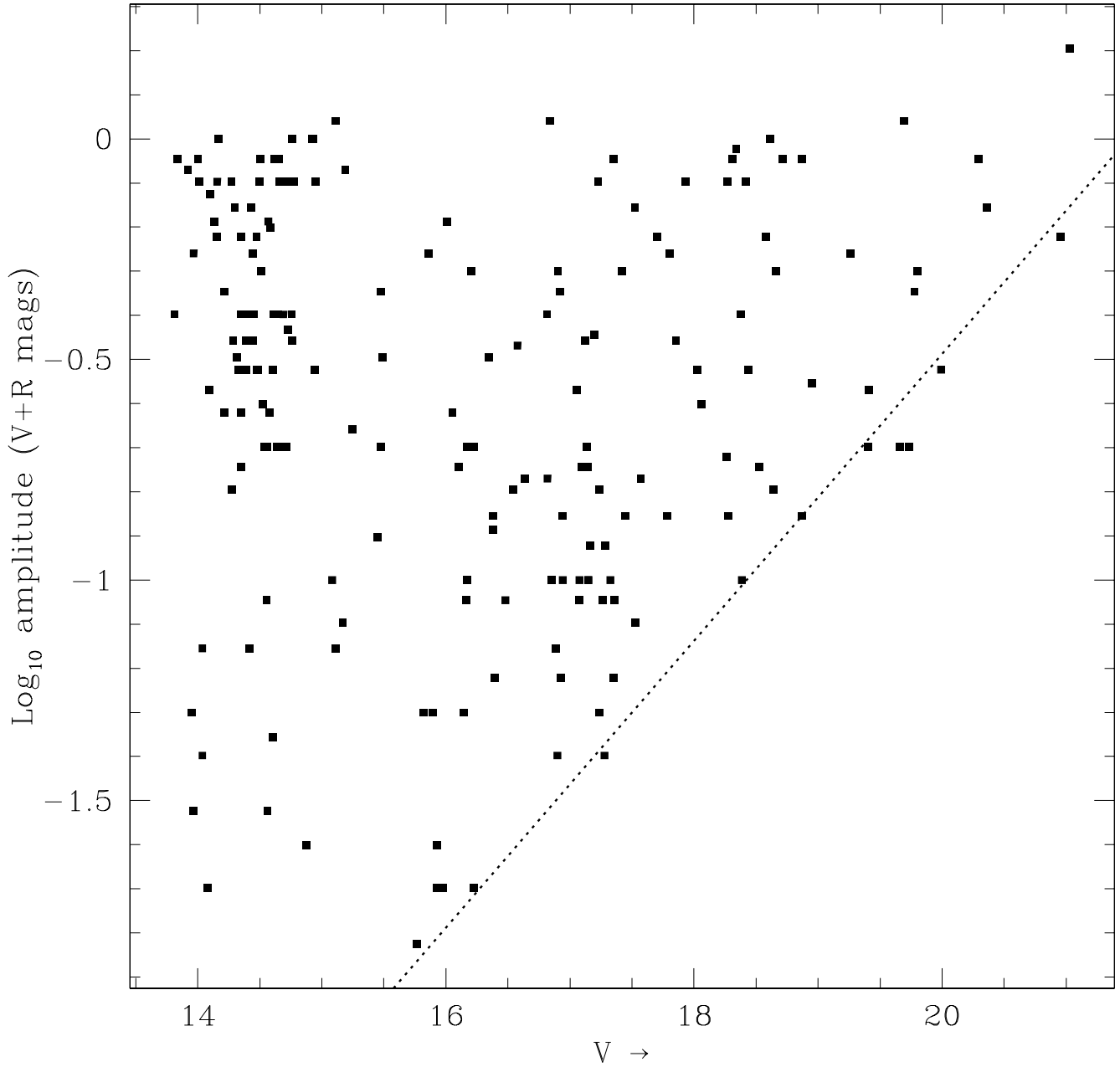


FIG. 8.— The logarithm of the total amplitude of each variable star (measured with the V+R filter), plotted as a function of corresponding V magnitude. This allows insight to be made into the detection limits of the variability search. It can be seen that the catalog detection limit is 0.015 magnitudes (1.5%) at $V \sim 16.0$. Therefore variables with total amplitude greater than or equal to this value at this magnitude can be detected. Similarly, at $V \sim 20.0$, the limit of detection is measured at ~ 0.3 magnitudes (33%), and represents the limits imposed by both the photometric uncertainty and the AoV variability detection method.

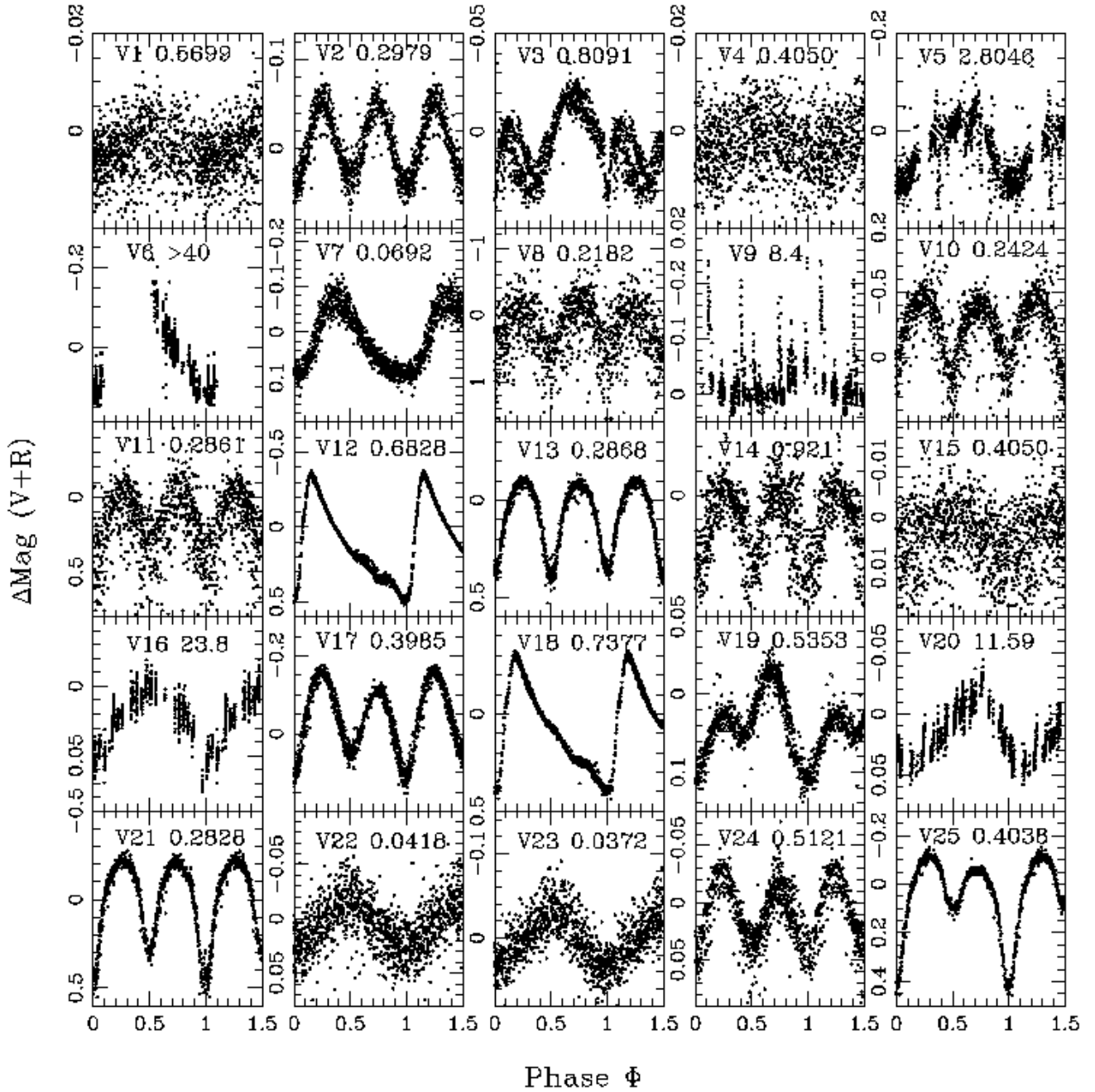


FIG. 9.— The phase-wrapped differential V+R magnitude lightcurves for all variable stars detected in the dataset, plotted in order of identification. The designation of each star and the respective period in days are also plotted.

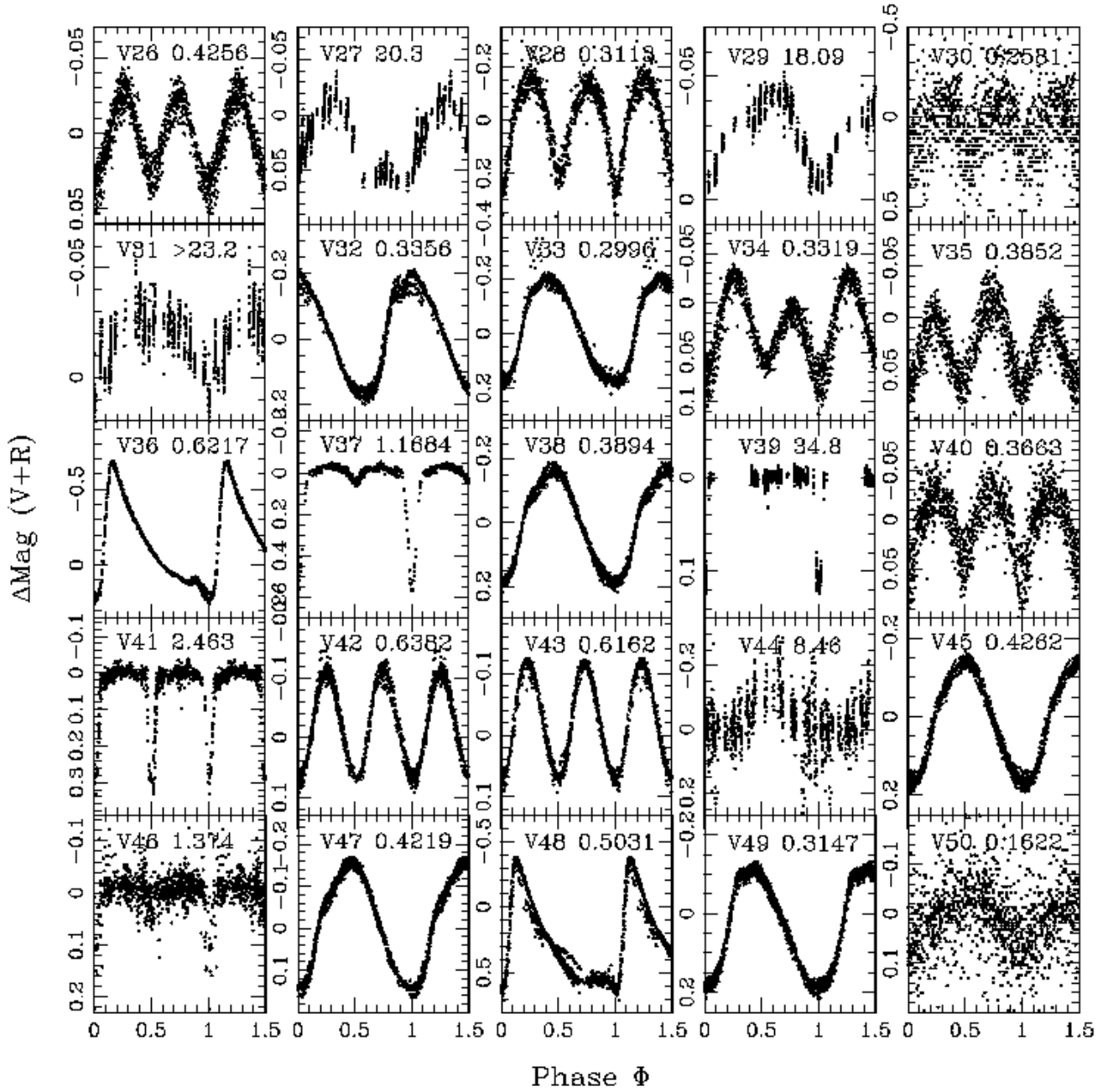


FIG. 10.— Phase-wrapped differential V+R magnitude variable star lightcurves (continued).

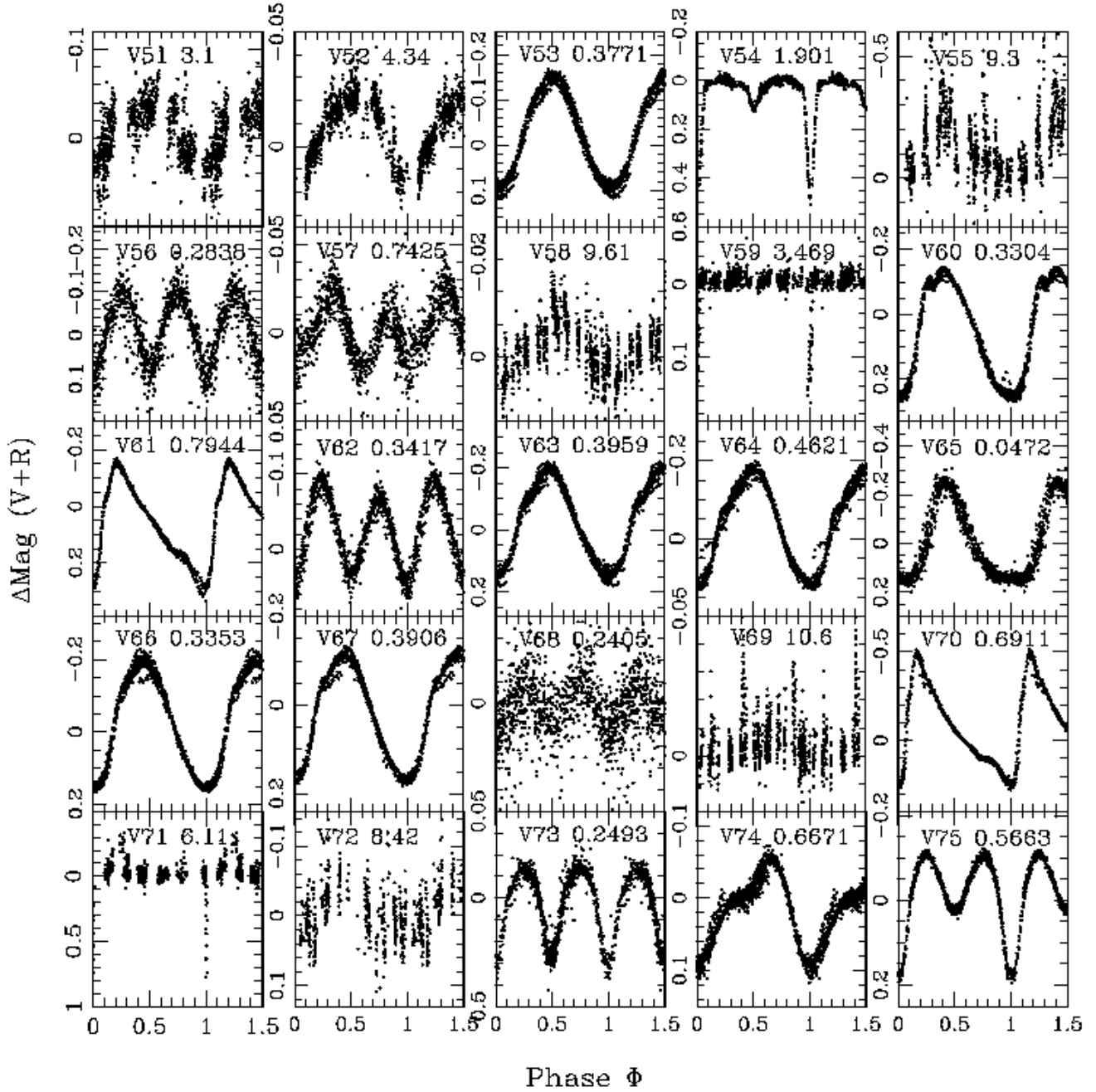


FIG. 11.— Phase-wrapped differential V+R magnitude variable star lightcurves (continued).

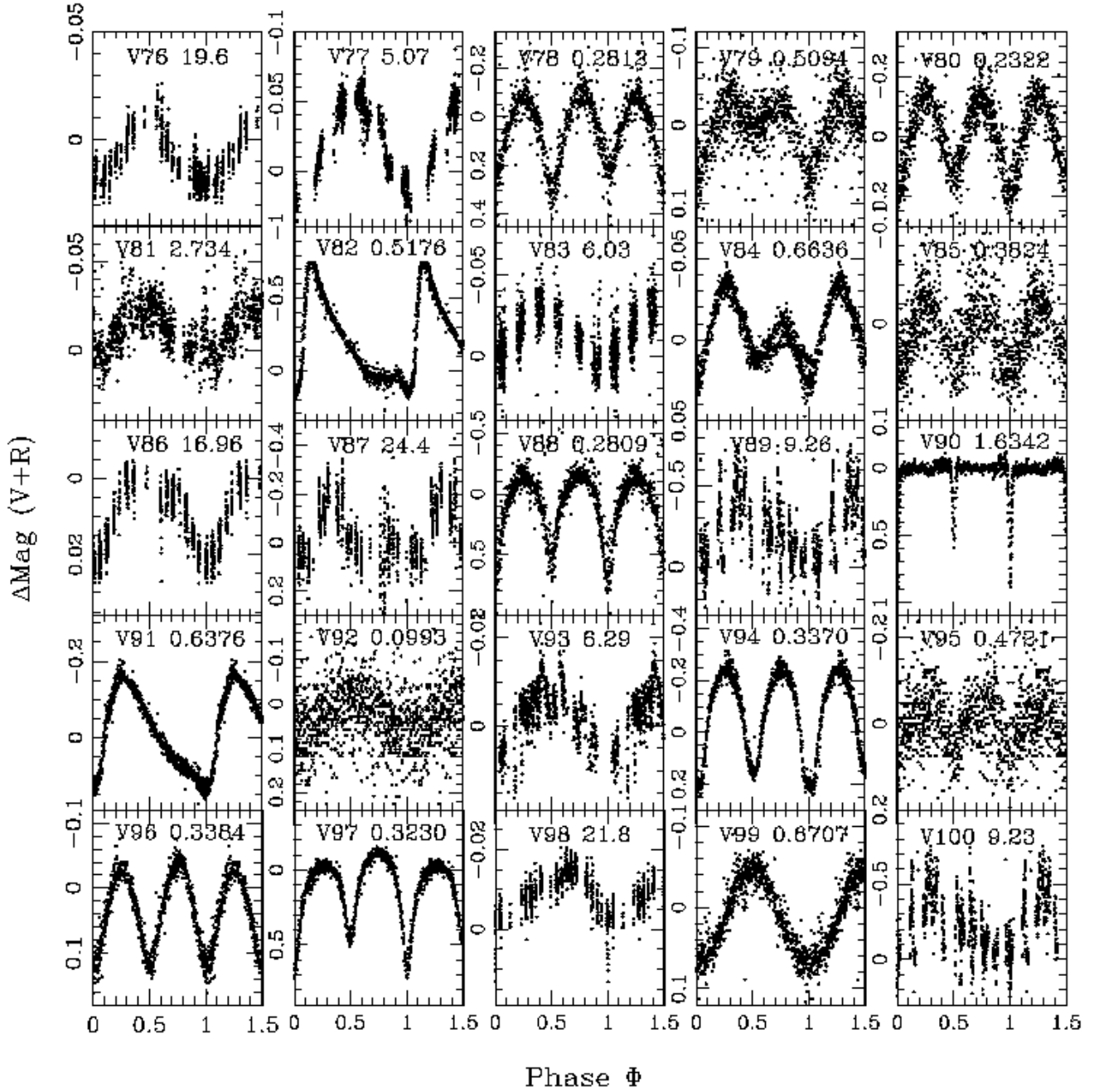


FIG. 12.— Phase-wrapped differential V+R magnitude variable star lightcurves (continued).

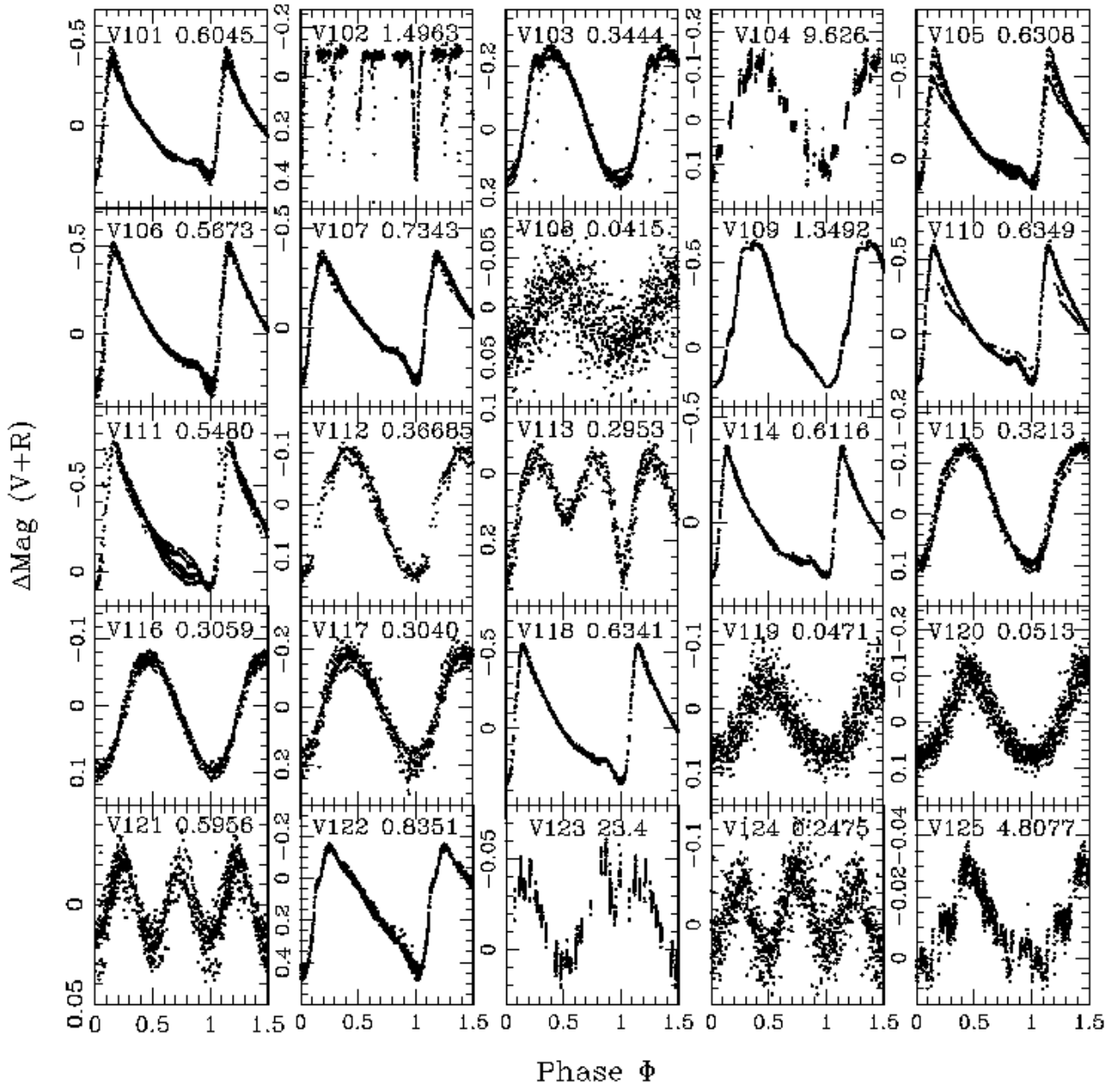


FIG. 13.— Phase-wrapped differential V+R magnitude variable star lightcurves (continued).

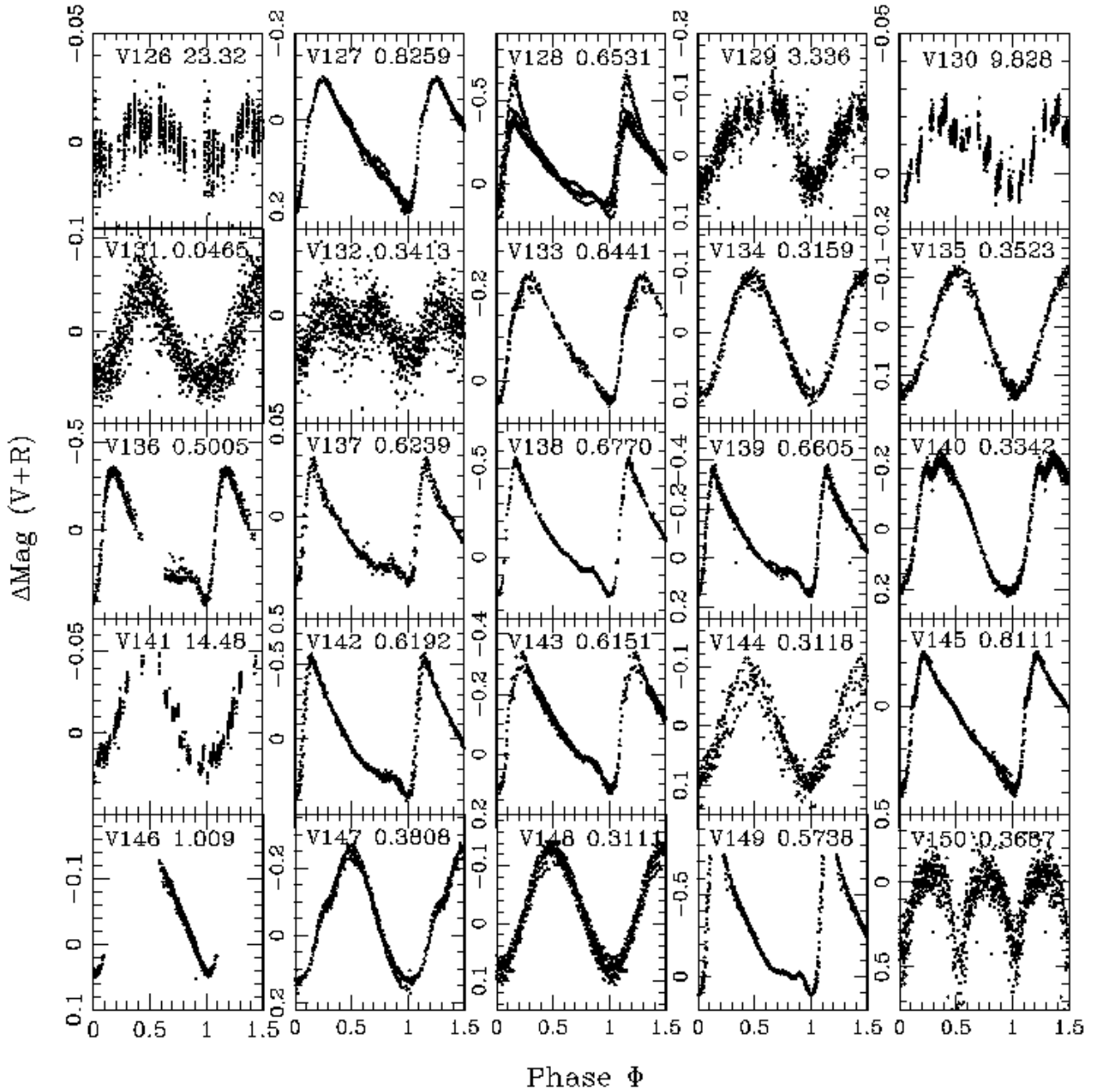


FIG. 14.— Phase-wrapped differential V+R magnitude variable star lightcurves (continued).

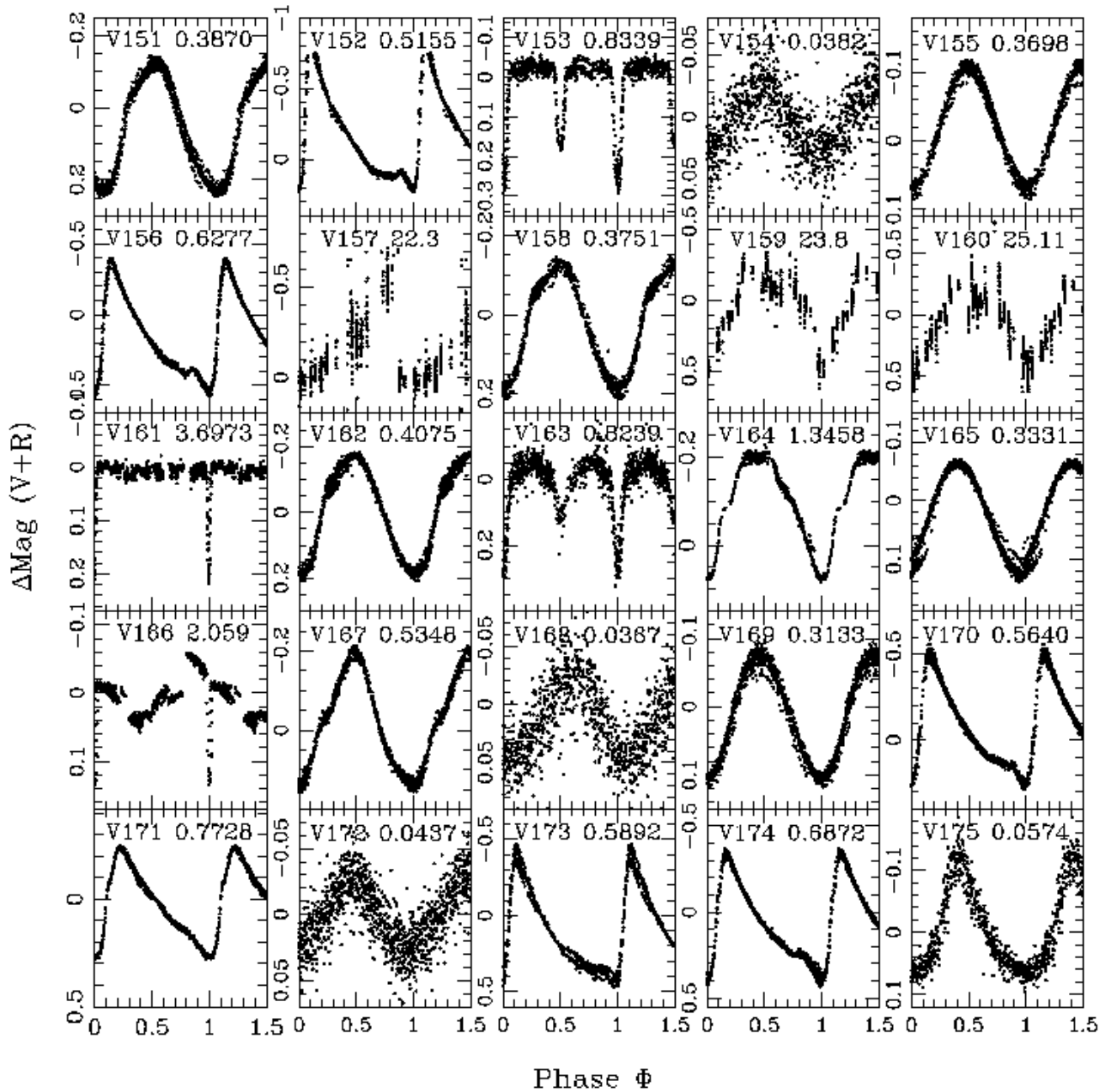


FIG. 15.— Phase-wrapped differential V+R magnitude variable star lightcurves (continued).

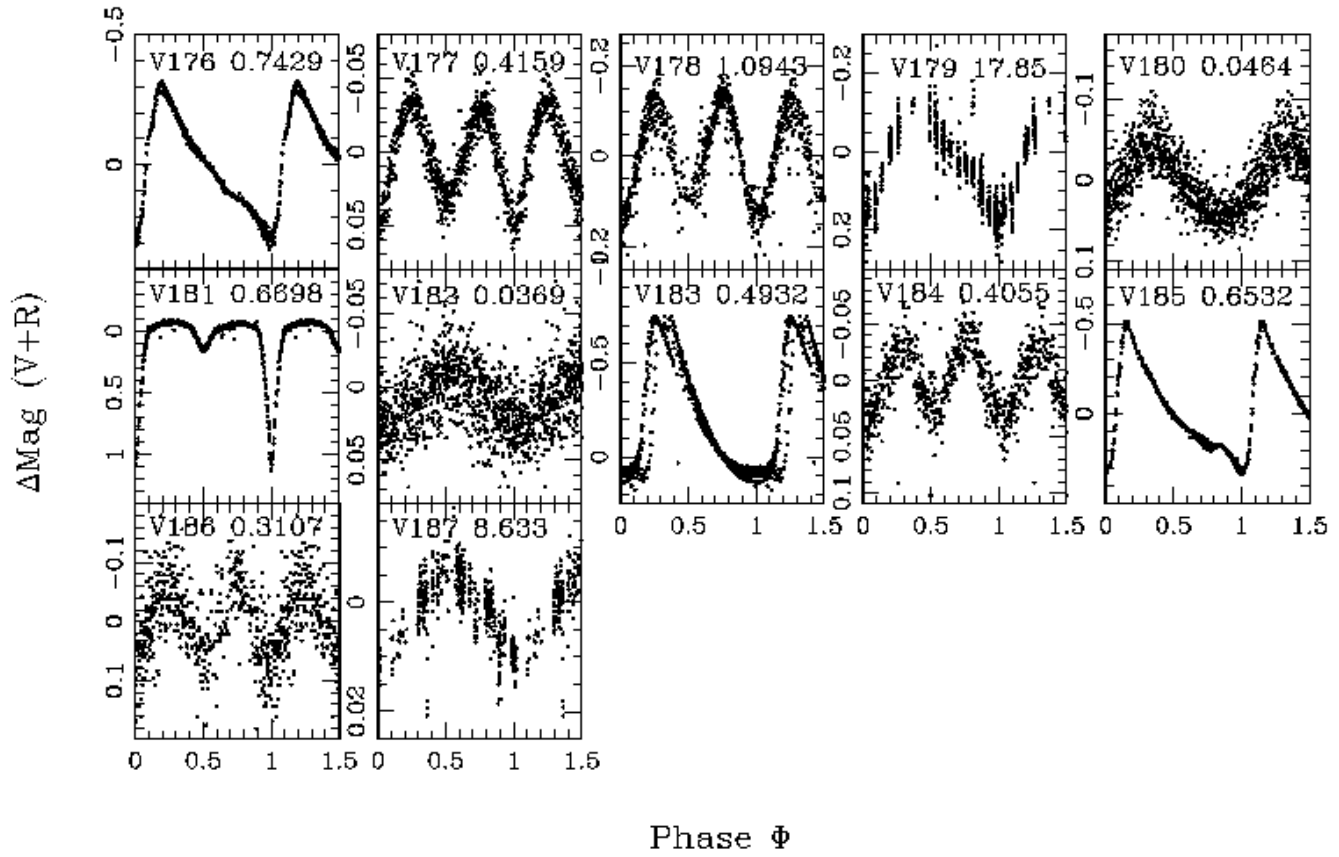


FIG. 16.— Phase-wrapped differential V+R magnitude variable star lightcurves (continued).

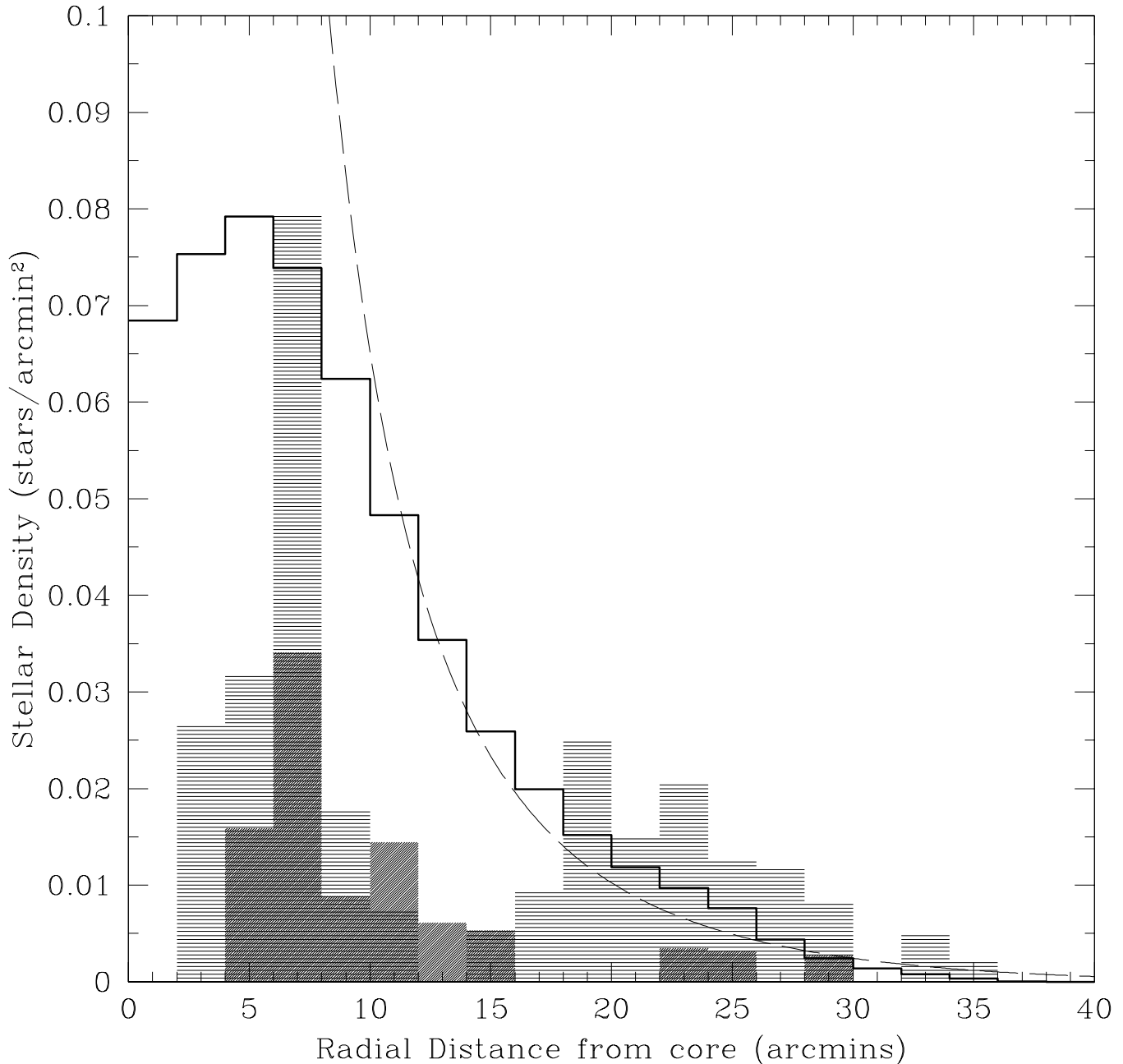


FIG. 17.— The radial distribution of eclipsing binary stars, plotted as binary density as a function of projected distance in arcminutes from the cluster core. The light histogram corresponds to the contact binaries ($P \leq 1d$) and the darker shading the detached binaries ($P > 1d$). There is no difference between the radial distribution of these different types of binary in the ω Cen field as indicated by a KS test. Also plotted is the total stellar population (open histogram) and the theoretical King profile using the parameters of Harris (1996). Our recovered stellar densities are complete to $R \sim 10'$. There appears to be a lack of binaries with radial distance $8' \rightarrow 15'$ in the cluster, perhaps indicating two separate populations.

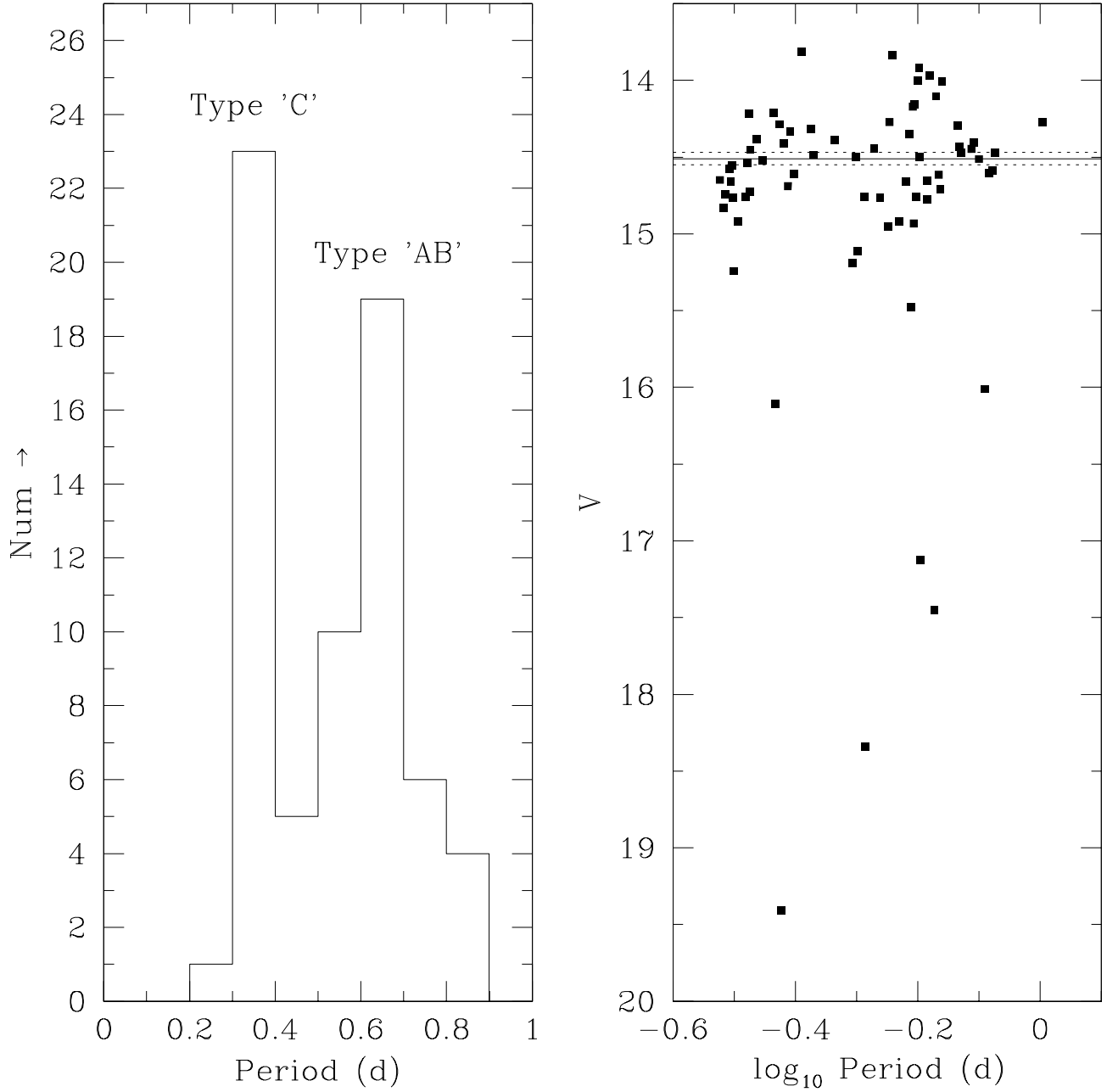


FIG. 18.— The period distribution of the detected RR Lyrae stars (left), and the corresponding period-magnitude diagram (right). Two main populations of RR Lyrae can be seen: the longer period Type ‘AB’ RR Lyrae and the shorter period Type ‘C’. The period-magnitude diagram shows that all the RR Lyrae are clustered around $V=14.51\pm 0.04$, strongly indicative of their membership in ω Cen. The shorter period Type ‘C’ RR Lyrae show somewhat less scatter around their mean than their longer period Type ‘AB’ counterparts. This is due to the ‘C’ RR Lyrae having smaller amplitudes, thus magnitudes of these stars at random phases are closer to their actual average magnitude. A number of RR Lyrae are seen running from $V\sim 16.0\rightarrow\sim 19.5$ and are attributed to background contamination from the Galactic Disk. No RR Lyrae are seen brighter than $V\sim 13.8$ as our time-series data are saturated there (see Fig. 1).

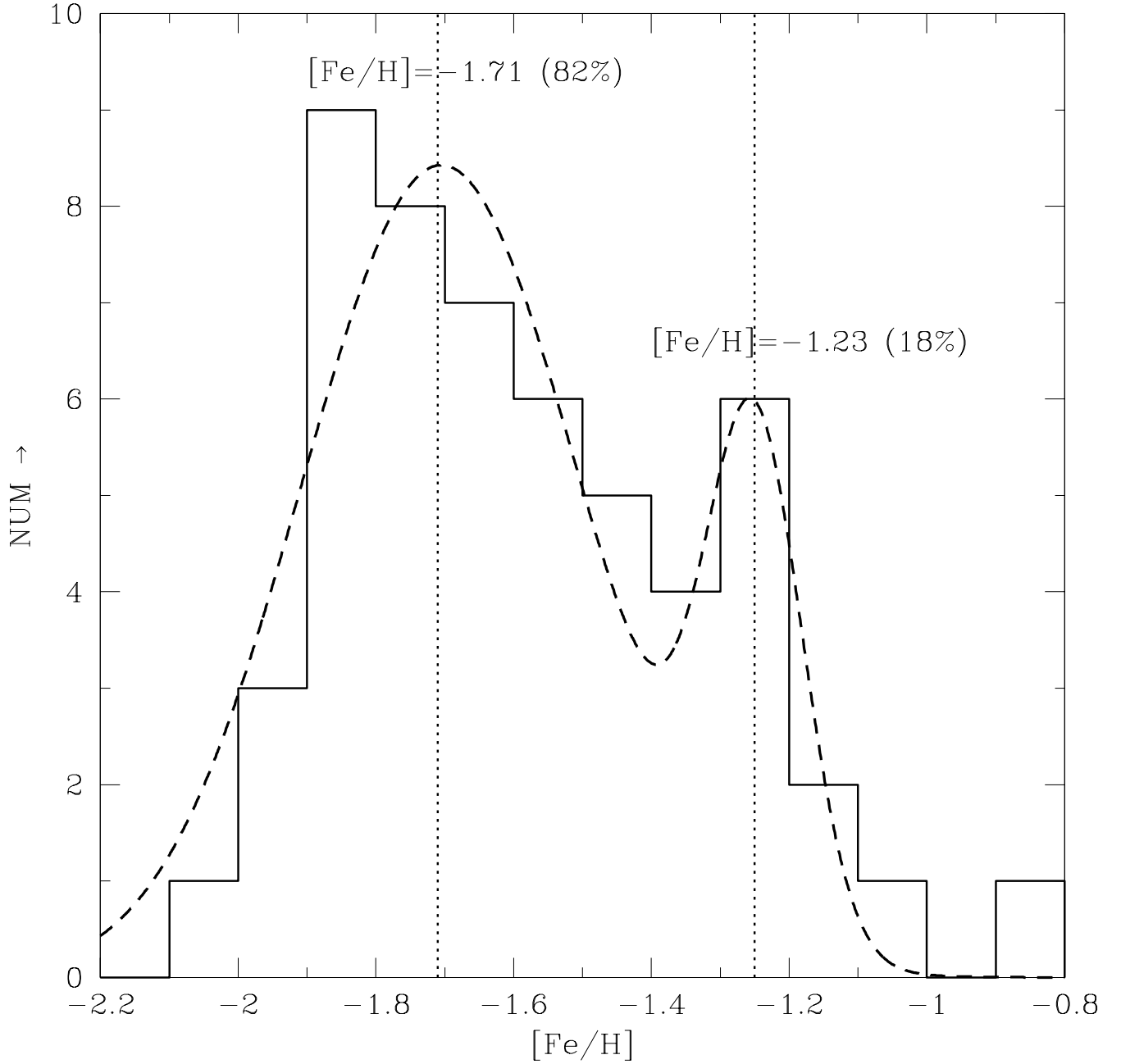


FIG. 20.— The distribution of $[Fe/H]$ for 53 of our RR Lyrae stars which could be crossidentified with those of Rey et al. (2000) (open histogram). Two Gaussian distributions have been fitted and their peak $[Fe/H]$ and relative fractions determined (overplotted), with a dispersion due to the natural dispersion of the sample and the error in the Rey et al. (2000) metallicity determinations. This $[Fe/H]$ distribution is assumed to apply to our total RR Lyrae sample and is used to determine the cluster distance modulus.

<i>CCD</i>	<i>RA(J2000.0)</i> h m s	<i>DEC(J2000.0)</i> ° ' "
1	13:28:05	-47:08:58
2	13:28:05	-47:21:52
3	13:28:05	-47:34:44
4	13:28:05	-47:47:43
5	13:25:34	-47:48:12
6	13:25:34	-47:35:06
7	13:25:34	-47:22:07
8	13:25:34	-47:08:57

Table 1: Equatorial coordinates (J2000.0) for the centres of the eight WFI CCDs.

<i>ID</i>	<i>Type</i>	<i>Period(d)</i>	<i>RA(J2000.0)</i> h m s	<i>DEC(J2000.0)</i> ° ' "	<i>V</i>	<i>V - I</i>	<i>PrevName</i>	
V1	Puls	0.569	13:29:03.20	-47:05:22.02	15.77	1.34	0.02	-
V2	EcB	0.298	13:29:02.31	-47:04:25.78	16.94	1.09	0.13	-
V3	EcB	0.809	13:29:02.16	-47:03:45.46	14.42	0.89	0.07	-
V4	Puls	0.405	13:28:53.93	-47:04:08.63	15.98	0.85	0.02	-
V5	LPV	2.805	13:28:26.68	-47:07:08.44	18.06	1.49	0.25	-
V6	LPV	>40	13:28:24.90	-47:14:47.07	14.94	2.80	≥0.35	-
V7	SX Phe	0.069	13:27:53.76	-47:13:18.45	16.17	0.56	0.2	-
V8	EcB	0.218	13:27:48.17	-47:07:27.80	21.03	1.60	1.4	-
V9	LPV	8.4	13:27:42.15	-47:12:31.77	16.94	0.97	0.08	-
V10	EcB	0.242	13:27:42.00	-47:07:24.15	20.29	1.46	0.90	-
V11	EcB	0.286	13:27:39.29	-47:09:26.64	20.36	1.57	0.70	-
V12	AB RR Lyr	0.683	13:27:32.83	-47:13:43.38	14.62	0.60	0.90	V149
V13	EcB	0.287	13:27:29.62	-47:13:09.65	17.42	1.03	0.50	-
V14	EcB	0.920	13:27:59.82	-47:13:12.57	16.40	1.07	0.05	-
V15	Puls	0.405	13:27:22.35	-47:11:12.86	15.92	0.94	0.01	-
V16	LPV	23.79	13:27:15.73	-47:13:10.13	16.16	1.07	0.09	-
V17	EcB	0.398	13:27:02.82	-47:08:49.08	16.34	0.43	0.35	V213
V18	AB RR Lyr	0.738	13:27:55.05	-47:04:38.51	14.43	0.77	0.70	V172
V19	Puls/EcB	0.535	13:29:00.98	-47:26:14.07	17.57	1.18	0.16	-
V20	LPV	11.59	13:28:59.41	-47:25:31.22	16.48	1.30	0.08	-
V21	EcB	0.283	13:28:53.83	-47:16:53.10	18.42	1.48	0.75	-
V22	SX Phe	0.041	13:28:53.57	-47:19:29.71	17.15	0.47	0.07	-
V23	SX Phe	0.037	13:28:44.57	-47:24:50.96	17.16	0.46	0.10	-
V24	EcB	0.512	13:28:35.26	-47:23:56.91	17.07	0.49	0.10	V255
V25	EcB	0.404	13:28:32.81	-47:26:24.32	17.71	0.95	0.55	V245
V26	EcB	0.426	13:28:25.94	-47:23:52.31	14.56	0.73	0.09	-
V27	LPV	20.3	13:28:25.03	-47:16:41.47	15.08	1.35	0.09	-
V28	EcB	0.311	13:28:18.70	-47:18:34.48	19.80	0.85	0.50	-
V29	LPV	18.09	13:28:23.48	-47:21:16.62	13.95	1.08	0.05	-
V30	EcB	0.258	13:29:09.27	-47:24:31.15	20.96	1.64	0.55	-
V31	LPV	23.25	13:27:43.09	-47:26:35.59	15.82	1.13	0.05	-
V32	C RR Lyr	0.336	13:27:35.61	-47:26:30.58	14.45	0.53	0.40	V82
V33	C RR Lyr	0.299	13:27:30.20	-47:28:05.37	14.65	0.49	0.40	V19
V34	EcB	0.332	13:27:28.71	-47:26:19.71	16.38	0.49	0.12	V240
V35	EcB	0.385	13:27:28.68	-47:27:39.28	16.38	0.41	0.11	V254
V36	AB RR Lyr	0.622	13:27:45.04	-47:24:56.84	14.93	0.82	0.90	V18
V37	S.Det.EcB	1.168	13:27:44.03	-47:26:09.56	14.13	0.39	0.60	V78
V38	C RR Lyr	0.779	13:27:36.64	-47:24:48.64	14.41	0.60	0.40	V81
V39	EcB	34.8*	13:27:42.06	-47:23:34.95	15.45	1.04	0.12	NV406
V40	EcB	0.366	13:27:36.20	-47:23:46.53	17.28	0.48	0.13	V241
V41	S.Det.EcB	2.463	13:27:21.72	-47:23:32.93	17.20	0.86	0.30	V212
V42	EcB	0.638	13:27:20.47	-47:23:59.38	14.64	0.51	0.20	V169
V43	EcB	0.616	13:28:03.46	-47:21:28.19	14.71	0.56	0.20	V289
V44	LPV	8.463	13:27:35.42	-47:21:08.44	18.03	0.76	0.20	-
V45	C RR Lyr	0.426	13:27:20.86	-47:22:06.03	14.49	0.68	0.35	V77
V46	EcB	0.687	13:27:19.48	-47:21:48.77	18.26	0.72	0.15	-
V47	C RR Lyr	0.422	13:27:19.65	-47:18:47.19	14.32	0.59	0.35	V75
V48	AB RR Lyr	0.503	13:27:07.22	-47:17:34.43	15.11	0.91	1.10	V74
V49	C RR Lyr	0.315	13:29:04.07	-47:36:21.78	14.76	0.57	0.30	V177
V50	Puls	0.162	13:29:00.54	-47:30:23.80	19.66	1.16	0.20	-
V51	LPV	3.102	13:29:00.27	-47:36:37.57	18.39	2.07	0.10	-
V52	LPV	4.337	13:28:59.84	-47:36:12.18	16.14	1.10	0.05	-
V53	C RR Lyr/EcB	0.377/0.754	13:28:54.73	-47:30:21.08	19.41	0.89	0.25	-
V54	S.Det.EcB	1.901	13:28:53.72	-47:37:35.04	15.86	0.52	0.50	-
V55	LPV	9.259	13:28:51.95	-47:38:07.15	18.66	0.75	0.40	-
V56	EcB	0.284	13:28:37.20	-47:34:28.95	18.95	1.00	0.24	V244
V57	EcB	0.743	13:29:05.37	-47:39:49.94	16.88	0.97	0.07	-
V58	LPV	9.608	13:29:07.01	-47:37:32.15	15.93	0.86	0.02	-
V59	Det.EcB	3.469	13:27:21.36	-47:39:31.43	16.82	1.02	0.16	-

The total variable star catalog. Tabulated are the identification number of each variable, its type, period in days, J2000.0 equatorial coordinate s, V magnitude and V-I color as intensity-averaged values measured from the CMD dataset, the V+R amplitude, the alternate name from Kaluzny et al. (2004) if the variable is previously known. Those variables marked with a ‘-’ in the Prev Name column are hence new discoveries. EcB refers to Eclipsing Binaries, with S.Det.EcB and Det.EcB referring to semi-detached and detached systems respectively. LPV denotes a long period variable. The periods marked with a * denote those systems which contain only one eclipse in the data and had their periods determined via the visible secondary ellipsoidal variations.

<i>ID</i>	<i>Type</i>	<i>Period(d)</i>	<i>RA(J2000.0)</i> h m s	<i>DEC(J2000.0)</i> ° ' "	<i>V</i>	<i>V - I</i>	<i>PrevName</i>	
V60	C RR Lyr	0.330	13:27:37.66	-47:37:35.21	14.76	0.61	0.40	V16
V61	AB RR Lyr	0.794	13:27:49.36	-47:36:50.78	14.51	0.70	0.50	V57
V62	EcB	0.342	13:27:21.77	-47:37:19.43	16.64	0.34	0.16	V214
V63	C RR Lyr	0.396	13:27:41.01	-47:34:08.19	14.61	0.70	0.40	V22
V64	C RR Lyr	0.462	13:27:38.29	-47:34:15.02	14.39	0.70	0.30	V24
V65	SX Phe	0.047	13:27:53.90	-47:31:54.39	16.92	0.30	0.40	V194
V66	C RR Lyr	0.335	13:27:45.99	-47:32:44.37	14.73	0.60	0.40	V105
V67	C RR Lyr	0.391	13:27:27.73	-47:33:43.18	14.33	0.55	0.30	V70
V68	EcB	0.241	13:27:22.95	-47:32:18.83	17.28	0.89	0.04	-
V69	LPV	10.64	13:27:08.59	-47:32:54.86	16.23	0.99	0.02	-
V70	AB RR Lyr	0.691	13:27:22.08	-47:30:12.69	14.01	-0.96	0.80	V102
V71	Det.EcB	6.110*	13:27:08.30	-47:31:41.54	17.35	0.90	0.80	-
V72	LPV	8.41	13:27:08.05	-47:31:39.83	18.87	0.90	0.12	-
V73	EcB	0.249	13:29:04.61	-47:50:31.04	18.58	0.80	0.50	-
V74	Puls	0.667	13:29:03.53	-47:48:58.30	16.54	1.05	0.16	-
V75	EcB	0.566	13:28:51.72	-47:48:19.06	15.49	0.50	0.30	-
V76	LPV	19.6	13:28:51.35	-47:52:48.95	15.89	1.07	0.05	-
V77	LPV	5.070	13:28:07.59	-47:53:03.78	16.17	0.97	0.10	-
V78	EcB	0.281	13:28:06.77	-47:45:33.73	19.27	1.16	0.40	V246
V79	EcB	0.509	13:28:06.34	-47:46:55.30	18.64	0.99	0.14	-
V80	EcB	0.232	13:27:57.01	-47:48:38.15	19.78	1.26	0.40	-
V81	LPV	2.733	13:27:38.59	-47:42:51.23	16.93	1.01	0.05	-
V82	AB RR Lyr	0.518	13:27:36.47	-47:46:40.07	18.34	0.76	0.90	V283
V83	LPV	6.033	13:27:35.03	-47:49:46.33	17.36	0.92	0.06	-
V84	EcB	0.664	13:27:27.23	-47:47:32.29	15.17	0.99	0.07	V282
V85	EcB	0.382	13:26:44.60	-47:51:12.54	18.28	0.87	0.12	-
V86	LPV	16.96	13:26:42.33	-47:47:49.67	14.56	0.92	0.03	-
V87	LPV	24.39	13:26:31.41	-47:53:59.42	16.20	0.94	0.50	-
V88	EcB	0.281	13:26:21.31	-47:52:49.21	19.69	1.44	1.10	-
V89	LPV	9.26	13:26:20.52	-47:50:04.12	18.31	0.83	0.80	-
V90	Det.EcB	1.634	13:26:18.70	-47:53:14.44	18.72	1.39	0.90	-
V91	AB RR Lyr	0.638	13:26:14.03	-47:53:08.18	17.12	0.77	0.35	-
V92	SX Phe	0.099	13:26:07.49	-47:47:16.85	19.73	1.11	0.15	-
V93	LPV	6.289	13:25:04.23	-47:50:52.73	13.97	0.86	0.02	-
V94	EcB	0.337	13:25:03.82	-47:49:32.58	17.81	0.83	0.50	-
V95	EcB	0.472	13:24:59.90	-47:48:32.27	19.99	2.14	0.20	-
V96	EcB	0.338	13:24:57.89	-47:43:36.97	17.14	0.79	0.18	-
V97	EcB	0.323	13:24:56.74	-47:49:28.98	18.27	1.20	0.85	-
V98	LPV	21.81	13:24:55.14	-47:49:17.78	14.08	0.91	0.02	-
V99	C RR Lyr/EcB	0.671/1.342	13:24:40.44	-47:45:22.52	17.45	0.98	0.18	-
V100	Det.EcB	9.232	13:24:36.22	-47:48:37.29	18.87	1.20	0.70	-
V101	AB RR Lyr	0.605	13:26:07.69	-47:37:55.74	14.66	0.77	0.80	V49
V102	Det.EcB	1.496	13:26:47.32	-47:35:58.83	16.91	0.51	0.50	V210
V103	C RR Lyr	0.344	13:26:02.12	-47:36:19.50	14.39	0.45	0.40	V64
V104	LPV	9.626	13:25:49.68	-47:37:00.26	17.05	1.33	0.30	NV384
V105	AB RR Lyr	0.631	13:26:12.24	-47:34:17.44	14.00	0.42	0.90	V115
V106	AB RR Lyr	0.567	13:26:22.35	-47:34:34.98	14.27	0.52	0.80	V44
V107	AB RR Lyr	0.734	13:26:07.14	-47:33:10.35	14.30	0.63	0.70	V34
V108	SX Phe	0.041	13:26:40.49	-47:33:45.12	17.27	0.54	0.09	V228
V109	TypeII Cep	1.349	13:26:35.69	-47:32:47.03	13.22	0.98	0.82	V60
V110	AB RR Lyr	0.635	13:26:30.29	-47:33:01.40	14.50	0.71	0.90	V122
V111	AB RR Lyr	0.548	13:26:25.48	-47:32:47.87	14.76	0.82	0.80	V120
V112	C RR Lyr	0.367	13:26:45.33	-47:30:37.99	14.21	0.75	0.22	V158
V113	EcB	0.295	13:26:41.76	-47:31:28.91	16.81	1.00	0.45	NV338
V114	AB RR Lyr	0.611	13:26:40.55	-47:30:17.31	14.35	0.65	0.70	V118
V115	C RR Lyr	0.321	13:26:39.64	-47:30:26.74	14.92	0.95	0.24	V48
V116	C RR Lyr	0.306	13:26:38.28	-47:31:16.53	14.74	0.59	0.20	V119
V117	C RR Lyr	0.304	13:26:28.15	-47:31:49.74	14.83	0.42	0.40	V121
V118	AB RR Lyr	0.634	13:26:24.52	-47:30:45.27	13.92	0.43	0.91	V40
V119	SX Phe	0.047	13:26:20.44	-47:31:58.92	17.09	0.60	0.19	V197

Table 2 (continued).

<i>ID</i>	<i>Type</i>	<i>Period(d)</i>	<i>RA(J2000.0)</i> h m s	<i>DEC(J2000.0)</i> ° ' "	<i>V</i>	<i>V - I</i>	<i>PrevName</i>	
V120	SX Phe	0.051	13:26:18.07	-47:30:34.81	16.05	0.90	0.24	NV324
V121	EcB	0.596	13:26:17.72	-47:30:22.77	14.57	0.53	0.06	NV357
V122	AB RR Lyr	0.835	13:26:17.57	-47:30:10.93	14.59	1.60	0.65	V128
V123	LPV	23.35	13:26:08.18	-47:30:31.79	15.12	1.09	0.07	V216
V124	EcB	0.248	13:26:08.18	-47:31:26.32	17.79	0.73	0.14	NV332
V125	LPV	4.808	13:25:31.89	-47:31:55.63	14.61	0.81	0.04	-
V126	LPV	23.32	13:25:21.47	-47:34:06.77	16.90	1.10	0.03	-
V127	AB RR Lyr	0.826	13:25:07.87	-47:36:54.11	14.61	0.81	0.30	V63
V128	AB RR Lyr	0.653	13:25:10.93	-47:37:33.52	14.65	0.74	0.90	V69
V129	LPV	3.336	13:24:58.54	-47:36:07.77	18.53	1.41	0.18	V284
V130	LPV	9.815	13:24:56.93	-47:32:28.83	14.04	1.04	0.04	-
V131	SX Phe	0.047	13:24:54.09	-47:41:03.53	17.24	0.73	0.14	-
V132	EcB	0.341	13:24:49.58	-47:33:30.42	17.22	1.02	0.04	-
V133	AB RR Lyr	0.844	13:26:41.09	-47:28:18.74	14.47	0.58	0.30	V144
V134	C RR Lyr	0.316	13:26:40.45	-47:26:36.85	15.25	1.43	0.20	V267
V135	C RR Lyr	0.352	13:26:39.93	-47:28:03.81	14.52	0.58	0.24	NV356
V136	AB RR Lyr	0.500	13:26:39.66	-47:26:55.80	14.50	0.26	0.75	V165
V137	AB RR Lyr	0.624	13:26:39.51	-47:27:04.97	14.16	0.44	0.07	V96
V138	AB RR Lyr	0.677	13:26:37.99	-47:27:36.86	14.10	0.68	0.80	V139
V139	AB RR Lyr	0.661	13:26:35.42	-47:28:05.63	13.97	0.61	0.55	V52
V140	C RR Lyr	0.334	13:26:31.72	-47:27:05.67	14.22	0.26	0.45	V137
V141	LPV	14.48	13:26:31.62	-47:27:26.01	14.04	0.99	0.07	NV386
V142	AB RR Lyr	0.619	13:26:26.77	-47:27:57.00	14.17	0.54	1.00	V62
V143	AB RR Lyr	0.615	13:26:26.22	-47:28:17.93	15.48	1.22	0.45	V27
V144	AB RR Lyr	0.312	13:26:43.18	-47:25:58.06	14.66	0.50	0.20	-
V145	AB RR Lyr	0.811	13:26:27.16	-47:24:47.36	16.01	2.11	0.75	-
V146	AB RR Lyr?	1.009?	13:26:13.21	-47:26:10.97	14.28	0.75	≥ 0.20	V263
V147	C RR Lyr	0.381	13:26:11.24	-47:26:00.03	14.41	-0.31	0.40	V21
V148	C RR Lyr	0.311	13:26:43.92	-47:22:49.09	14.58	0.51	0.24	V274
V149	AB RR Lyr	0.574	13:26:42.81	-47:24:22.63	13.83	0.34	0.90	V51
V150	S.Det.EcB	0.369	13:26:33.44	-47:23:01.03	17.23	0.53	0.80	V205
V151	C RR Lyr	0.387	13:26:27.29	-47:24:07.39	14.69	0.66	0.40	V12
V152	AB RR Lyr	0.515	13:26:18.39	-47:23:13.33	14.76	0.67	1.00	V5
V153	Det.EcB	0.834	13:26:17.40	-47:23:17.76	16.58	0.19	0.32	V209
V154	SX Phe	0.038	13:26:14.44	-47:23:54.75	17.36	0.49	0.08	V227
V155	C RR Lyr/EcB	0.370/0.740	13:26:13.17	-47:24:04.54	16.10	-0.15	0.20	V58
V156	AB RR Lyr	0.628	13:26:12.99	-47:24:19.81	14.76	0.77	1.00	V4
V157	LPV	22.3	13:26:12.20	-47:24:37.74	17.52	1.31	≥ 0.65	-
V158	C RR Lyr	0.375	13:26:07.04	-47:24:37.49	14.29	0.48	0.35	V10
V159	LPV	23.82	13:26:05.67	-47:23:54.47	17.93	0.84	0.80	-
V160	LPV	25.11	13:26:03.80	-47:23:36.83	18.61	0.81	0.90	-
V161	Det.EcB	3.697*	13:26:38.87	-47:21:40.61	16.22	0.99	0.22	NV409
V162	C RR Lyr	0.407	13:26:33.17	-47:22:26.01	13.82	-0.03	0.40	V66
V163	S.Det.EcB	0.823	13:26:22.79	-47:21:43.44	17.85	0.84	0.35	NV363
V164	TypeII Cep	1.346	13:26:14.86	-47:21:15.17	14.09	0.82	0.27	V92
V165	C RR Lyr	0.333	13:26:04.07	-47:21:47.22	14.54	0.53	0.16	V185
V166	EcB	2.059	13:26:38.55	-47:20:00.09	14.67	0.82	0.20	NV378
V167	AB RR Lyr	0.535	13:26:12.79	-47:19:36.27	14.45	0.68	0.35	V68
V168	SX Phe	0.039	13:26:08.40	-47:19:24.65	17.15	0.52	0.09	V219
V169	C RR Lyr	0.313	13:25:49.44	-47:20:21.88	14.56	0.46	0.20	V163
V170	AB RR Lyr	0.564	13:26:28.60	-47:18:47.39	14.95	0.73	0.80	V67
V171	AB RR Lyr	0.773	13:26:23.53	-47:18:48.25	14.45	-1.42	0.50	V54
V172	SX Phe	0.044	13:26:11.19	-47:17:54.05	17.08	0.50	0.08	V218
V173	AB RR Lyr	0.589	13:25:30.83	-47:27:21.21	14.92	0.78	1.00	V45
V174	AB RR Lyr	0.687	13:25:30.21	-47:25:51.91	14.71	0.79	0.80	V46
V175	SX Phe	0.057	13:25:01.16	-47:25:29.69	17.14	0.58	0.20	V196
V176	AB RR Lyr	0.743	13:25:06.56	-47:23:33.70	14.47	0.73	0.60	V85
V177	EcB	0.416	13:25:02.08	-47:24:15.45	16.86	0.59	0.09	V248
V178	EcB	1.094	13:25:19.22	-47:22:31.05	18.44	1.01	0.30	V235
V179	LPV	17.85	13:25:00.42	-47:17:39.99	18.38	1.24	0.35	-
V180	SX Phe	0.046	13:26:38.93	-47:11:51.28	17.10	0.59	0.13	V202
V181	S.Det.EcB	0.669	13:26:20.53	-47:04:27.64	16.84	1.00	1.10	-
V182	SX Phe	0.037	13:26:17.27	-47:11:49.95	17.52	0.57	0.05	V232
V183	AB RR Lyr	0.493	13:26:09.94	-47:13:40.04	15.19	0.84	0.80	V130
V184	EcB	0.406	13:25:15.77	-47:03:54.87	17.33	0.90	0.07	-
V185	AB RR Lyr	0.653	13:25:13.28	-47:12:28.64	14.77	0.78	0.80	V134
V186	EcB	0.311	13:24:45.29	-47:09:17.90	19.40	0.96	0.20	-
V187	LPV	8.63	13:24:36.96	-47:07:32.53	14.88	0.95	0.03	-

Table 2 (continued).